MOLECULAR AND CELLULAR BIOLOGY, Jan. 2003, p. 636–644 Vol. 23, No. 2
0270-7306/03/$08.00+0 DOI: 10.1128/MCB.23.2.636–644.2003

Chondromodulin I Is a Bone Remodeling Factor

Yuko Nakamichi,[1,2] Chisa Shukunami,[3] Takashi Yamada,[1,4] Ken-ichi Aihara,[1] Hirotaka Kawano,[4] Takashi Sato,[1,5] Yuriko Nishizaki,[3] Yoko Yamamoto,[1] Masayo Shindo,[1] Kimihiro Yoshimura,[1] Takashi Nakamura,[1] Naoyuki Takahashi,[2] Hiroshi Kawaguchi,[4] Yuji Hiraki,[3] and Shigeaki Kato[1,5]*

The Institute of Molecular and Cellular Biosciences,[1] and The Department of Orthopedic Surgery, Faculty of Medicine,[4] University of Tokyo, Bunkyo-ku, Tokyo, The Institute for Oral Science, Matsumoto Dental University, Hiro-oka, Shiojiri, Nagano[2], The Institute for Frontier Medical Sciences, Kyoto University, Sakyo-ku, Kyoto,[3] and CREST, Japan Science and Technology, Kawaguchi, Saitama,[5] Japan

Received 10 May 2002/Returned for modification 11 July 2002/Accepted 21 October 2002

Chondromodulin I (ChM-I) was supposed from its limited expression in cartilage and its functions in cultured chondrocytes as a major regulator in cartilage development. Here, we generated mice deficient in ChM-I by targeted disruption of the *ChM-I* gene. No overt abnormality was detected in endochondral bone formation during embryogenesis and cartilage development during growth stages of ChM-I$^{-/-}$ mice. However, a significant increase in bone mineral density with lowered bone resorption with respect to formation was unexpectedly found in adult ChM-I$^{-/-}$ mice. Thus, the present study established that ChM-I is a bone remodeling factor.

Endochondral bone development during embryogenesis and longitudinal bone growth in growing vertebrates require continuous cartilage growth (18). Proliferating chondrocytes originate from a region of resting chondrocytes, differentiate first into prehypertrophic chondrocytes and then into hypertrophic chondrocytes able to secrete the cartilage matrix. Through invasion by blood vessels, the calcified cartilage and vascular matrix are gradually replaced by bone matrix with the recruitment of osteoclasts and osteoblasts that mediate bone resorption and formation and eventual bone remodeling (1, 30). Thus, in bone growth, blood vessel invasion into cartilage is pivotal to the process of endochondral bone formation.

Distinct classes of factors are thought to play cognate roles in the spatiotemporal regulation of the complicated yet sequential processes of cartilage differentiation and bone formation, particularly in angiogenic events. Fibroblast growth factor-2 (5, 31), transforming growth factor β (3), and vascular endothelial growth factor (4) are expressed in cartilage and have been identified as strong angiogenic agents. However, these factors are also present in avascular cartilage and in surrounding vascular regions. These findings raise the possibility that the actions of angiogenic factors may be suppressed by the inhibitory action of a specific factor in avascular cartilage. While tissue inhibitors of matrix metalloproteinase 1 and 2 have been identified from cartilage as possible angiogenesis inhibitors, they are also expressed in other tissues (20). The search for a cartilage-specific inhibitor of angiogenesis led to the identification of chondromodulin I (ChM-I), initially isolated from bovine epiphyseal cartilage as a factor with growth-promoting activity on cultured chondrocytes (10). ChM-I was found to be a potent stimulator of proteoglycan synthesis in growth plate chondrocytes and of chondrocyte colony formation in agarose (12). However, ChM-I inhibited cultured vascular endothelial cell tube morphogenesis and growth (8, 9). Thus, the physiological significance of ChM-I during endochondral bone formation as a bifunctional factor of chondrocyte growth and angiogenesis inhibition was suggested from distinct lines of evidence in vitro (27). However, due to the lack of mice deficient in ChM-I, there has been no information regarding the physiological role of ChM-I.

In the present study, we disrupted the murine *ChM-I* gene by homologous recombination to generate *ChM-I* knockout (*ChM-I*$^{-/-}$) mice. Homozygous *ChM-I*$^{-/-}$ mice were born without overt abnormalities and grew normally. Unexpectedly, *ChM-I*$^{-/-}$ mice exhibited no aberrations in endochondral bone formation during embryogenesis or in cartilage development during growth stages. However, a significant increase in bone mineral density was observed in 12-week-old *ChM-I*$^{-/-}$ mice. Analyses of bone formation and resorption indicators revealed that bone minerals accumulated in *ChM-I*$^{-/-}$ mice due to lowered bone resorption with respect to formation. Thus, our study revealed that the physiological role of ChM-I appears to be involved in the stimulation of bone remodeling through control of osteoclast and osteoblast functions rather than in cartilage development in intact animals.

MATERIALS AND METHODS

Gene targeting. A TT2 embryonic stem (ES) cell (34) genomic library was screened with a mouse ChM-I cDNA probe (24). A 9-kb fragment of mouse ChM-I containing the coding exons 1 to 3 was used to construct a targeting vector. A stop mutation was introduced at the beginning of the ChM-I coding region, and 3.5-kb fragment containing exon 3 was replaced with a phosphoglycerate kinase-neomycin cassette. TT2 ES cells were transfected with a linearized targeting vector (25 μg per 1.0×10^7 cells) by using a Bio-Rad Gene Pulser II at 250 V and 500 μF and grown under G418 selection as described previously (23, 36). Targeted ES cell clones were identified by Southern blot analysis with probe A and probe NEO (Fig. 1A) and were aggregated with CD-1 single 8-cell embryos to generate chimeras as described previously (23, 36). Chimeras were crossed with C57BL/6 female mice to produce germ line transmission of the targeted allele. Offspring were genotyped either by Southern blotting with probe A or by PCR with the three specific primers P1 (5′-TTGGTTGATGCTTCAG

* Corresponding author. Mailing address: The Institute of Molecular and Cellular Biosciences, University of Tokyo, 1-1-1 Yayoi, Bunkyo-ku, Tokyo 113-0032, Japan. Phone: 81-3-5841-8478. Fax: 81-3-5841-8477. E-mail: uskato@mail.ecc.u-tokyo.ac.jp.

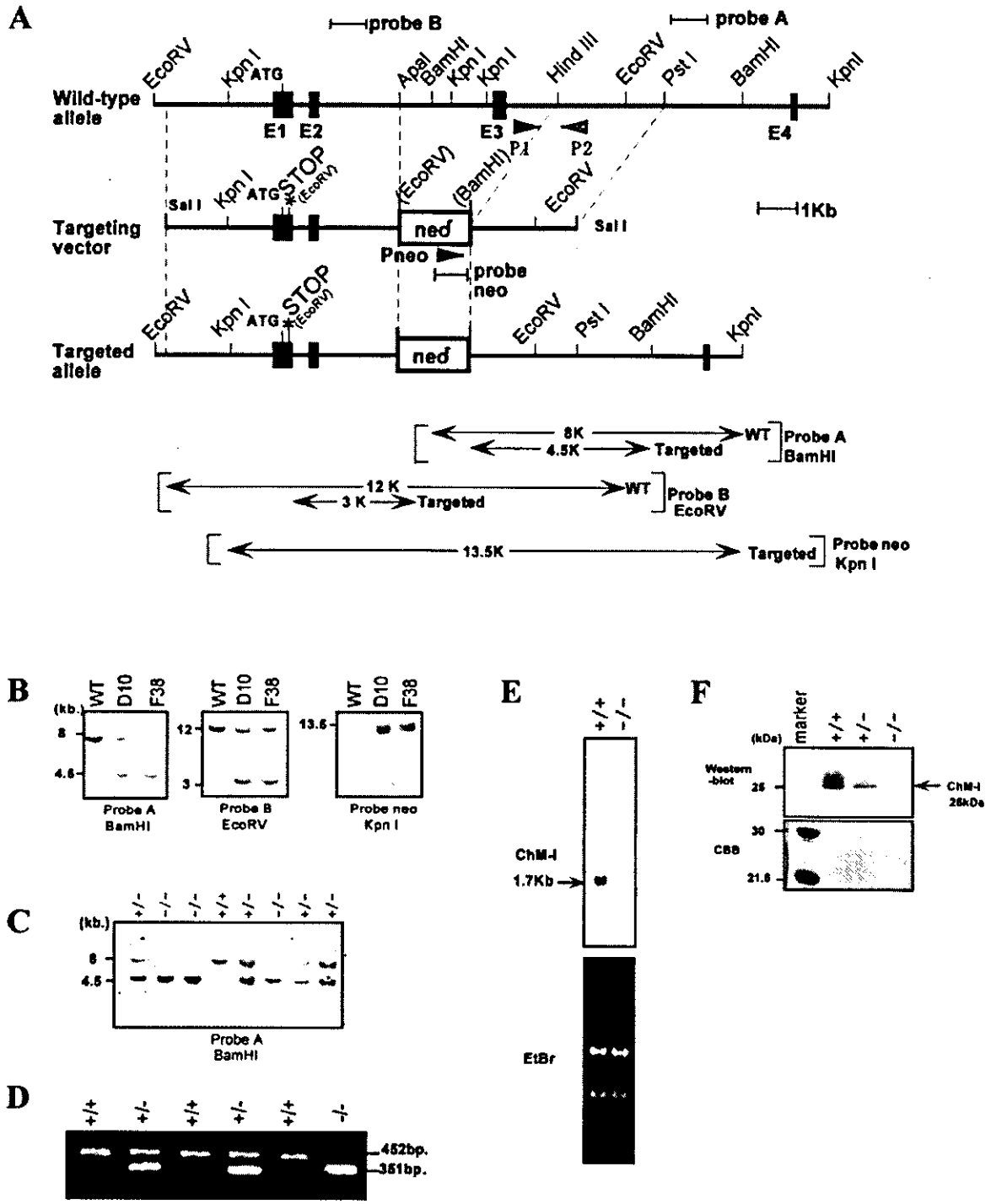

FIG. 1. Disruption of the mouse ChM-I gene. (A) Schematic representation of the *ChM-I* gene locus (top), gene targeting vector (middle), and the recombinated locus (bottom).The digested fragments detected by probe A, probe B, and probe NEO are indicated by bars. (B) Southern blot analysis of targeted ES clones. The targeting frequency was 0.3%. The presence of the 4.5-kb *Bam*HI fragment indicates proper targeting of the ChM-I locus, and the 3-kb *Eco*RV fragment indicates the introduction of the stop mutation. (C) Southern blot analysis of tail DNA from the offspring of heterozygous mates with probe A as described for panel B. (D) PCR genotyping of embryos at e13.5 of heterozygous matings with three primers (P1, P2, Pneo) as indicated in panel A. Primer 1 and primer 2 were used to detect the wild-type (WT) allele (amplification of a 452-bp fragment). Primer 2 and primer NEO were used to detect the targeted allele (amplification of a 351-bp fragment). (E) Northern blot analysis of RNA from *ChM-I*$^{+/+}$ and *ChM-I*$^{-/-}$ mice in the top panel. The bottom panel shows ethidium bromide (EtBr) staining of the RNA used. (F) Western blot analysis confirming the absence of ChM-I protein with an anti-rhChM-I polyclonal antibody. The top panel shows the immunoreactivity after hybridization with anti-ChM-I antibody. The bottom panel shows Coomassie brilliant blue staining of the SDS-polyacrylamide gel electrophoresis gel.

TGTG-3'), P2 (5'-CTTGTGCACAGACCAGAACAA-3'), and Pneo (5'-CCG CTTCCTCGTGCTTTACGG-3'). Temperature cycling conditions were as follows: denaturation at 95°C for 2 min followed by 35 cycles of 95°C for 1 min, 54°C for 1 min, and 72°C for 1.5 min.

Northern blot analysis. Total RNA was prepared from rib cartilage of 3- to 4-week-old *ChM-I*$^{+/+}$ or *ChM-I*$^{-/-}$ mice by a single-step method (35). Total RNA (15 μg) was separated by electrophoresis on a 1% agarose formaldehyde gel and transferred onto a Nytran filter with Turboblotter (Schleicher and Schuell). The filter was then hybridized with a ^{32}P-labeled probe that is an 822-bp *Eco*RI fragment from nucleotides 628 to 1449 of the ChM-I cDNA. After hybridization, the filter was washed at 55°C for 30 min in 1× SSPE (1× SSPE is 0.18 M NaCl, 10 mM NaH_2PO_4, and 1 mM EDTA [pH7.7])–0.1% sodium dodecyl sulfate (SDS) once, then washed at 55°C for 30 min in 0.1× SSPE–0.1% SDS twice. The filter was exposed to BIOMAX film (Eastman Kodak) at −80°C.

Western blot analysis. Whole ribs from 3-week-old mice were homogenized in extraction buffer {20 mM MES [2-(*N*-morpholino)ethanesulfonic acid]-NaOH [pH 6.0], 0.1 M aminocaproate, 6 M guanidium chloride} at 4°C and centrifuged at 10,000 × *g*. The supernatant was diluted with 2 volumes of distilled water and applied to a butyl-toyopearl 650 affinity column OSOH. The column was washed three times with distilled water. Bound proteins were eluted by 70% ethanol and dried. The dried materials (8 μg) were dissolved in Laemmli buffer, electrophoresed by SDS–15% polyacrylamide gel electrophoresis, and blotted onto an Immobilon-P membrane (Millipore). Bands that were immunoreactive with an anti-ChM-I polyclonal antibody for the C-terminal peptides of the mature form of human ChM-I, corresponding to the Asp^{252} to Val^{334} residues, which is a highly conserved region among species (26), were stained by using enhanced chemiluminescence methods (Amersham Biosciences).

Morphology and histological analyses. For cleared skeletal preparations (23), embryos from embryonic day 13.5 (e13.5) were fixed in 99.5% ethanol for 4 days and transferred to acetone. After 3 days, they were rinsed with water and stained for 10 days in a staining solution consisting of 1 volume of 0.1% Alizarin red S (Sigma) in 95% ethanol, 1 volume of 0.3% Alcian blue 8GX (Sigma) in 70% ethanol, 1 volume of 100% acetic acid, and 17 volumes of ethanol. After rinsing with 96% ethanol, specimens were kept in 20% glycerol–1% KOH at room temperature until the skeletons became clearly visible. For hematoxylin-fast green-safranin O staining, bones were fixed in 4% paraformaldehyde overnight and decalcified in Morse's solution (10% [wt/vol] sodium citrate, 22.5% [vol/vol] formic acid) overnight prior to embedding in paraffin. For Villanueva Goldner, toluidine blue, and tartartic acid resistance alkaline phosphatase (TRAP) staining, tibiae were embedded in glycolmethacrylate without decalcification (36) (see below).

Bone radiographic analysis and histomorphometry. For radiographic analysis, femora from male weight-matched mice were dissected free of soft tissues and subjected to radiographic analysis with a soft X-ray apparatus (model CMB-2; SOFTEX) (36). Bone mineral density was measured by dual energy X-ray absorptiometry with a bone mineral analyzer (PIXImus2; GE Medical Systems). For in vivo fluorescent labeling (21), a single intraperitoneal injection of calcein (1.6 mg/kg of body weight) was administrated at days 0 and 4. Mice were sacrificed at day 5. Tibiae were fixed in 99.5% ethanol and embedded in glycolmethacrylate without decalcification. Longitudinal serial sections (7 μm thick) were prepared with a microtome (model 2050; Reichert Jung). The sections were stained with Villanueva Goldner to discriminate between mineralized and unmineralized bone and to identify cellular components (36). Images were visualized by fluorescent microscopy. Histomorphometry of bone sections was performed for at least eight optical fields of the secondary spongiosa with a semiautomated system for bone analysis (Osteoplan II; Carl Zeiss) at 200-fold magnification (17). All sections were examined blind. Nomenclature, symbols, and units are those recommended by the Nomenclature Committee of the American Society for Bone and Mineral Research (22).

Reverse transcription-PCR analysis. For the isolation osteoblasts for primary culture, calvaria from newborn C57BL/6 mice were dissected into pieces with scissors and cultured in α-minimal essential medium (α-MEM) containing 10% heat-inactivated fetal bovine serum (FBS) at 37°C in 5% CO_2. After the cells were grown to subconfluence, total cellular RNA was extracted as previously described (35). Femora and tibiae were dissected free of adherent tissues and epiphyseal cartilage, and the bone marrow was flushed out. The total RNA of the bone was prepared from several mice (12-week-old mice). For isolation of osteoclasts, primary calvarial osteoblasts (1.5×10^6 cells/dish) and bone marrow cells (10^7 cells/dish) were cocultured in α-MEM supplemented with 10% FBS, 1α,25-dihydroxy vitamin D_3 (10^{-8} M) and prostaglandin E_2 (10^{-6} M) in 100-mm-diameter dishes precoated with type I collagen gel (cell matrix type-IA; Nitta Gelatin) (28). Osteoclasts were formed within 7 days in the coculture, and differentiated osteoclasts were collected as described previously (16). The purified osteoclasts in this preparation were subjected to total RNA extraction. First-strand cDNA was synthesized from total RNA with oligo(dT)$_{12-18}$ primer with the Super Script II preamplification system (Life Technologies) and subjected to PCR amplification with Ex *Taq* polymerase (TaKaRa) and the specific pair of primers mChM-If (in exon 5) (5'-CTTAAGCCCATGTATCCAAA-3') and mChM-Ir (in exon 7) (5'-CCAGTGGTTCACAGATCTTC-3'). Temperature cycling conditions were as follows: denaturation at 96°C for 3 min followed by 30 cycles of 96°C for 30s, 60°C for 1 min, and 72°C for 30s.

In vitro osteoclastogenesis. Bone marrow macrophages were isolated from whole tibial bone marrow of 12-week-old mice (n = 3) and cultured in α-MEM containing 10% heat-inactivated FBS at 37°C in 5% CO_2 (16). After 24 h in culture, the nonadherent cells were collected and replaced in a 96-well plate (2×10^5 cells/well) in α-MEM supplemented with 10% heat-inactivated FBS at 37°C in 5% CO_2 in the presence of 100 ng of recombinant human macrophage colony-stimulating factor (rhM-CSF) (leukoprol; Kyowa Hakko Kogyo)/ml. Cells were stimulated with 100 ng of soluble recombinant human receptor activator of nuclear factor-κB ligand (rhRANKL; Pepro Teck EC Ltd.)/ml on day 4 in the presence of 100 ng of rhM-CSF/ml. Cells were fixed and stained for TRAP as described previously (29) on day 9 or 10. TRAP-positive multinucleated cells containing three or more nuclei were counted as osteoclasts under microscopic examination. The results were expressed as the means ± standard deviations of four wells.

Serum and urinary indicators. Blood from 12-week-old male mice was collected by heart puncture under nembutal (Dainippon Pharmaceutical Co.) anesthesia. The levels of calcium, phosphorus, and alkaline phosphatase activity in serum were measured by using a calcium HR kit (Wako), inorganic phosphorus II kit (Wako), and liquitech alkaline phosphatase kit (Roche Diagnostic), respectively, with an autoanalyzer (type 7170; Hitachi) (36). The levels of osteocalcin in serum were measured by using the competitive radioimmunoassay kit by Biomedical Technologies, Inc. The urinary excretion of deoxypyridinoline cross-links, a marker of bone resorption (32), was measured in urine samples by using the Pyriliks-D enzyme-linked immunosorbent assay (Metra Biosystems). Results were expressed in nanomoles per millimole of urinary creatinine (Cr), as measured by a standard colorimetric technique with an autoanalyzer (type 7170; Hitachi).

RESULTS

Generation of targeted ChM-I-null mice. We disrupted the murine *ChM-I* gene in ES cells by homologous recombination to generate *ChM-I*$^{-/-}$ mice. The targeting vector (Fig. 1A) was constructed to introduce a stop codon at Cys-21, and a 3.5-kb genomic fragment containing exon 3 was replaced by a phosphoglycerate kinase-neomycin cassette. No overt abnormalities were found in *ChM-I*$^{+/-}$ mice, and crossbreeding of *ChM-I*$^{+/-}$ mice produced normal numbers of pups of all three possible genotypes (Fig. 1C) with the expected Mendelian distribution (61 +/+ mice, 128 +/− mice, and 56 −/− mice, for a total of 245 offspring) (Fig. 1B and C). Northern blot analysis of rib cartilage from normal mice with a cDNA probe encoding the mature form of ChM-I protein detected a single 1.7-kb transcript. No transcripts were found in *ChM-I*$^{-/-}$ mice, confirming the disruption of the *ChM-I* gene (Fig. 1E). Western blot analysis of whole-rib extracts from *ChM-I*$^{-/-}$ mice with an antibody against the mature ChM-I protein also confirmed the absence of the ChM-I protein (Fig. 1F).

ChM-I is not required for cartilage development and endochondral bone formation. *ChM-I*$^{-/-}$ mice grew normally with no discernible physical defects and with normal fertility. As ChM-I had been implicated in cartilage development, endochondral bone formation, and morphogenesis of the eye, careful histological examination of these tissues from *ChM-I*$^{-/-}$ mouse embryos and mice at various growth stages was performed. However, we failed to defect any abnormalities in cartilage formation (Fig. 2A), first ossification (Fig. 2B) in *ChM-I*$^{-/-}$ fetuses, and secondary ossification in *ChM-I*$^{-/-}$

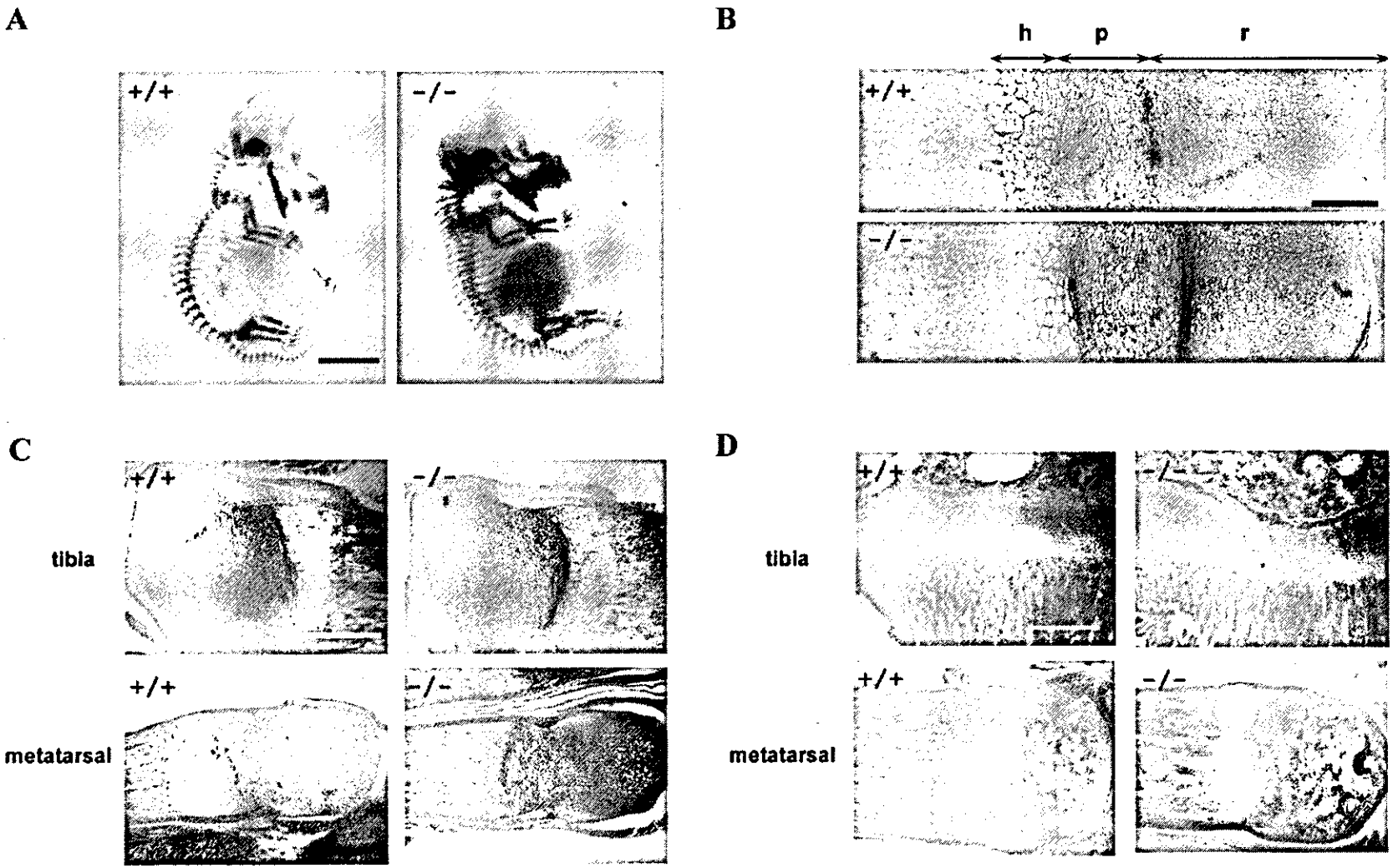

FIG. 2. No abnormality in cartilage development and endochondral bone formation of *ChM-I*$^{-/-}$ mice. (A) Alizarin red and Alcian blue staining of e13.5 embryos. Bar, 2 mm. (B) Safranin O-fast green-hematoxylin staining of proximal growth plate of tibiae from e18.5 embryos. Bar, 0.1 mm. h, hypertrophic zone; p, proliferating zone; r, resting zone. (C) Safranin O-fast green-hematoxylin staining of epiphyses from 1-week-old mice. Bar, 0.5 mm. (D) Safranin O-fast green-hematoxylin staining of epiphyses from 3-week-old mice. Bar, 0.5 mm. In all panels, no overt difference was detected between *ChM-I*$^{+/+}$ and *ChM-I*$^{-/-}$ mice.

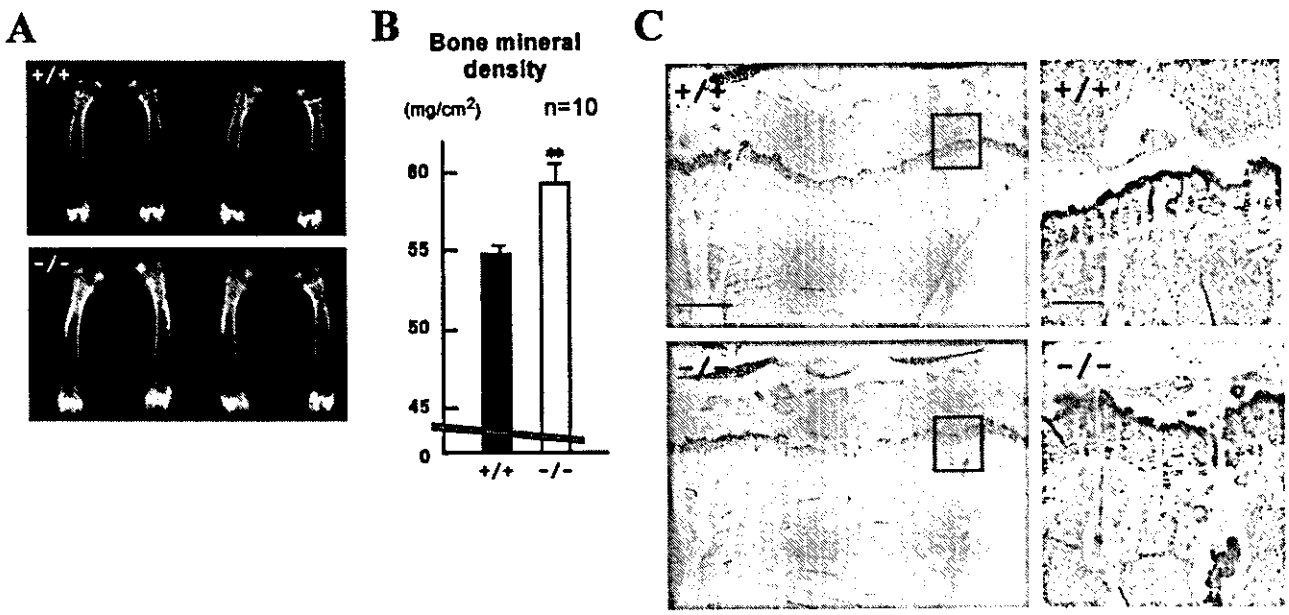
A
+/+
-/-
B
Bone mineral density
(mg/cm²)
n=10
60
55
50
45
0
+/+
-/-
C
+/+
-/-

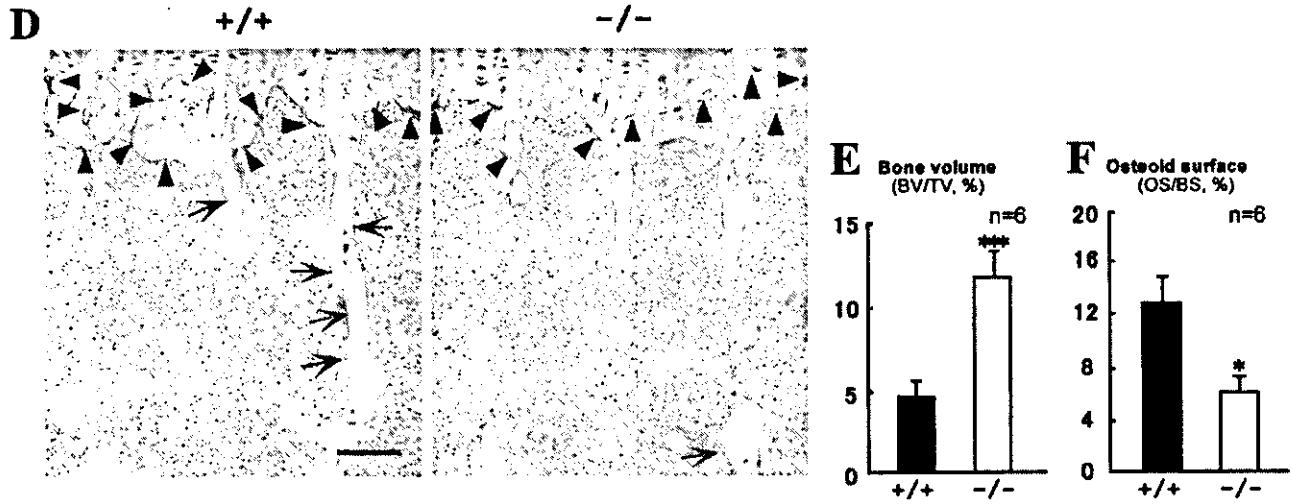
D
+/+
-/-
E
Bone volume
(BV/TV, %)
n=6
15
10
5
0
+/+
-/-
F
Osteoid surface
(OS/BS, %)
n=6
20
16
12
8
4
0
+/+
-/-

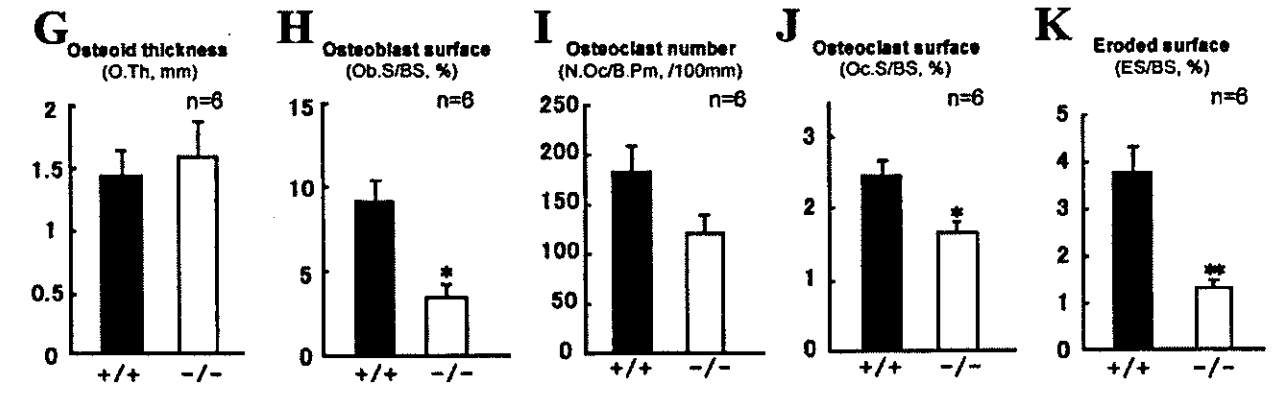
G
Osteoid thickness
(O.Th, mm)
n=6
2
1.5
1
0.5
0
+/+
-/-
H
Osteoblast surface
(Ob.S/BS, %)
n=6
15
10
5
0
+/+
-/-
I
Osteoclast number
(N.Oc/B.Pm, /100mm)
n=6
250
200
150
100
50
0
+/+
-/-
J
Osteoclast surface
(Oc.S/BS, %)
n=6
3
2
1
0
+/+
-/-
K
Eroded surface
(ES/BS, %)
n=6
5
4
3
2
1
0
+/+
-/-

mice at 1 and 3 weeks old (Fig. 2C and D), in agreement with normal growth of *ChM-I*$^{-/-}$ mice.

Mice homozygous for the ChM-I mutation exhibit increased bone mineral density. Unexpectedly, a significant increase in bone mineral density was observed in 12-week-old *ChM-I*$^{-/-}$ mice but not in *ChM-I*$^{+/-}$ mice. Also, the radiographic mineral density of the femur in mutant mice was approximately 10% higher than in wild-type mice (Fig. 3A and B). Histomorphometric analyses confirmed that trabecular bone volumes (bone volume per tissue volume) in mutant mice were 2.5-fold higher than in wild-type mice (Fig. 3C and E). However, no significant differences in bone or body size and shape were observed between *ChM-I*$^{-/-}$ and wild-type mice. Osteoid surfaces (osteoid surface per bone surface) in mutant mice were 54% lower than in wild-type mice (Fig. 3F), but the osteoid thickness value in mutant mice was equivalent to that in wild-type mice (Fig. 3G). Indeed, the expression of the ChM-I gene was detected in the primary culture osteoblasts and total bone, though their expression levels appear to be much lower than those in cartilage (Fig. 4).

As it was possible that the observed increase in bone mineral density was related to bone remodeling (2), we studied bone formation and resorption in terms of osteoblast and osteoclast function. TRAP-positive mature osteoclast and chondroclast numbers were reduced in *ChM-I*$^{-/-}$ mice (Fig. 3D). This was in agreement with the results of histomorphometry analyses that showed that the numbers of bone osteoclasts (osteoclast number per bone perimeter) and surface osteoclasts (osteoclast surface per bone surface) in *ChM-I*$^{-/-}$ mice were 33 and 34% lower than in wild-type mice, respectively (Fig. 3H and I). Eroded surface (eroded surface per bone surface) values, which represent osteoclast activity, were also significantly decreased in *ChM-I*$^{-/-}$ mice (Fig. 3J). In addition, osteoblast surface (osteoblast surface per bone surface) values, a reliable histomorphometric indicator of active osteoblast numbers, were significantly reduced to approximately 60% by *ChM-I* inactivation (Fig. 3K). Reflecting the reduced osteoclast and/or chondroclast activity in *ChM-I*$^{-/-}$ mice, more cartilaginous matrix remained in the first spongiosa of tibiae in the *ChM-I*$^{-/-}$ mice than in wild-type mice (Fig. 3C, right).

Loss of ChM-I affects bone metabolism. We then estimated the bone formation rate directly by using calcein double-labeling of the mineralized matrix (22). Both the mineral apposition rate (MAR) and bone formation rate (BFR) (BFR per bone surface) were significantly decreased in *ChM-I*$^{-/-}$ mice (Fig. 5A, B, and C). Reduced levels in serum of markers for osteoblastic function (alkaline phosphatase activity and osteocalcin) (Fig. 5E and F) and no alteration in serum minerals (Fig. 5G, H) supported the hypothesis that bone formation activity was reduced by *ChM-I* inactivation. Total urinary deoxypyridinoline levels, a marker of bone resorption, were measured by enzyme-linked immunosorbent assay; however, no statistical difference was observed between wild-type and *ChM-I*$^{-/-}$ mice (Fig. 5D). Moreover, in vitro osteoclastogenesis with donor bone marrow macrophages from mutant and wild-type mice revealed that *ChM-I* inactivation appears to cause no abnormality in osteoclastogenesis (Fig. 6). Our results indicated that the increased bone mineral density in *ChM-I*$^{-/-}$ mice appeared to be due to lowered bone resorption with respect to bone formation. Thus, the present study established that ChM-I is likely to be a bone remodeling factor rather than being involved in chondrocyte development.

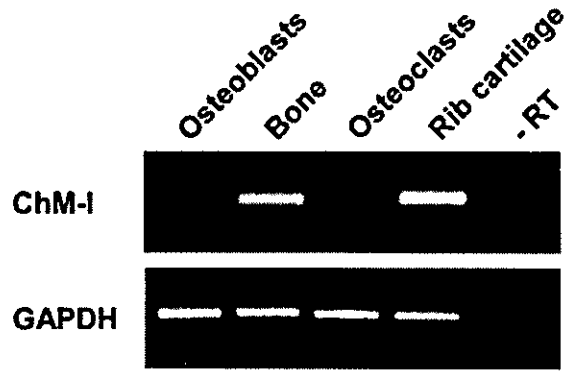

FIG. 4. ChM-I mRNA expression in bone. The top panel shows the ChM-I transcripts. The bottom panel shows glyceraldehydes-3-phosphate dehydrogenase (GAPDH) transcripts. Primary calvarial osteoblasts from newborn wild-type mice were cultured as described in Materials and Methods. Bones from wild-type 12-week-old mice were prepared as described in Materials and Methods. Osteoclasts were purified from coculture bone marrow cells with calvarial osteoblasts. Rib cartilage from 4-week-old wild-type mice was dissected free of adherent soft tissues. Reverse transcription-PCRs performed in the absence of reverse transcriptase (−RT) failed to detect any transcripts (representative lane shown).

FIG. 3. Increased bone mineral density in *ChM-I*$^{-/-}$ mice (12 weeks of age). (A and B) Radiological analyses of femora. (A) Plain X-ray images of femora. (B) Bone mineral density of femora measured by dual-energy X-ray absorptiometry. Bars represent means ± standard errors for wild-type (black bars) and mutant (white bars) mice. **, $P < 0.01$ between the two groups. Statistical differences between groups were assessed by Student's *t* test. (C and D) Histological analyses of proximal tibiae. (C) Undecalcified plastic sections were stained with toluidine blue, which stains cartilage violet and bone clear. The panels on the right are higher magnifications of the boxed areas in the panels on the left. Bars, 0.5 mm (left) and 0.1 mm (right). (D) Undecalcified plastic sections were stained with TRAP, which stains mature chondroclasts (arrowheads) and osteoclasts (arrows) red. Bar, 0.1 mm. (E to K) Static bone histomorphometric analyses of trabecular bones in proximal tibiae from 12-week-old mice. (E) Percent bone volume per tissue volume (BV/TV) represents the ratio of bone volume to tissue volume and estimates bone mass. Percent osteoid surface per bone surface (OS/BS) (F) and osteoid thickness (O.Th) (G) represent the proportion and thickness of bone surface covered with unmineralized matrix, respectively. (H) Percent osteoblast surface per bone surface (Ob.S/BS) represents the proportion of bone surface covered with osteoblasts. Osteoclast number per bone perimeter (N.Oc/B.Pm) (I) and percent osteoclast surface per bone surface (Oc.S/BS) (J) estimate bone resorption as osteoclast number and surface, respectively, divided by bone surface. (K) Eroded surface represents the function of osteoclasts. ES/BS, eroded surface per bone surface. Bars represent means ± standard errors for wild-type (black bars) and mutant (white bars) mice. Asterisks indicate statistically significant differences between the two groups. *, **, and *** indicate *P* values of <0.05, <0.01, <0.005, respectively.

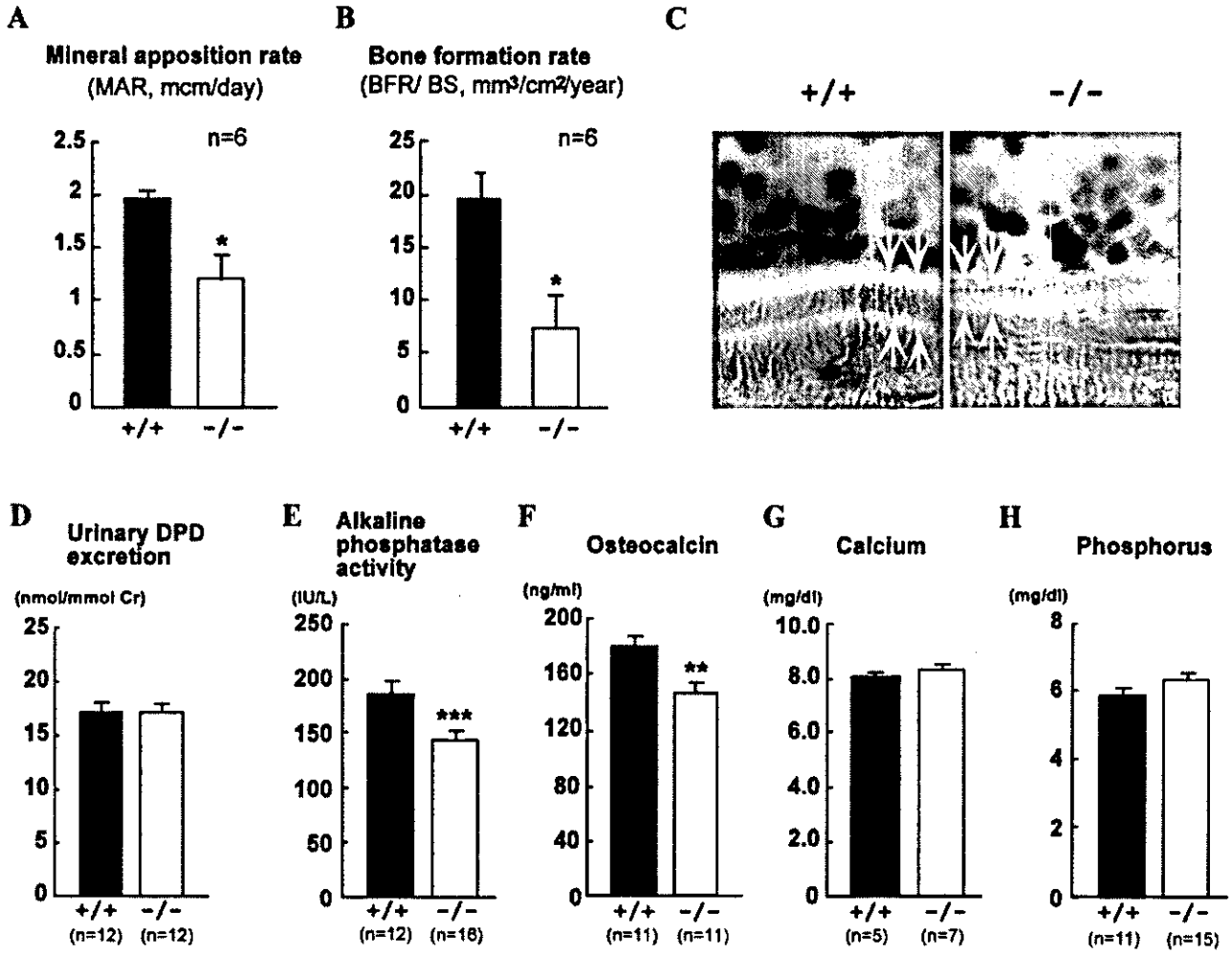

FIG. 5. Dynamic histomorphometric and serum biochemical parameters of bone metabolism in *ChM-I*$^{+/+}$ and *ChM-I*$^{-/-}$ mice (12 weeks of age). MAR (A) and BFR (B) are using sections from animals that were double-labeled with calcein in vivo. MAR and BFR measure the amount of bone that is mineralized or deposited per time unit and are based on the measurement of the distance between the two fluorescent labels. (C) Two calcein-labeled mineralization fronts of tibiae trabecular bones from *ChM-I*$^{+/+}$ and *ChM-I*$^{-/-}$ mice were visualized by fluorescent micrography. (D) Urinary deoxypyridinoline (DPD) excretion in 12-week-old wild-type and *ChM-I*$^{-/-}$ mice. (E) Alkaline phosphatase activity in serum. (F) Osteocalcin level in serum. (G) Calcium level in serum. (H) Phosphorus level in serum. Bars represent means ± standard errors for wild-type (black bars) and mutant (white bars) mice. Asterisks indicate statistically significant differences between the two groups (*, $P < 0.05$; **, $P < 0.01$, ***, $P < 0.005$).

DISCUSSION

ChM-I is a 25-kDa glycoprotein generated from a larger transmembrane precursor after posttranslational modification and proteolytic cleavage at a processing signal site (10). ChM-I was originally purified from bovine epiphyseal cartilage as a growth factor that stimulated anchorage-independent growth of chondrocytes in agarose (8) and induced proteoglycan synthesis (8). However, ChM-I also possesses inhibitory activity on the growth and tube morphogenesis of cultured vascular endothelial cells. Due to its bifunctional activities in vitro, it was thought that ChM-I might play a pivotal role in endochondral bone development during embryogenesis and in postnatal cartilage growth in vivo (27). However, our present observations with *ChM-I*$^{-/-}$ mice showed that ChM-I was not essential for normal cartilage formation and development. Indeed, our study revealed that ChM-I is more likely to be involved in normal bone remodeling, probably through regulating osteoclast and osteoblast numbers and functions. Detailed analysis of bones from *ChM-I*$^{-/-}$ mice showed that bone resorption was lower in comparison to bone formation, leading to increased bone mineral density and insufficient bone turnover.

Considering the marked cartilage phenotypes of mice deficient for angiogenic factors (6, 11, 33) or their inhibitors (7, 14), with which ChM-I was considered an equally potent factor in the cell culture systems (8, 9), the normal development of cartilage at embryonic and postnatal stages in *ChM-I*$^{-/-}$ mice was unexpected. Furthermore, no overt abnormalities were found in tests for rib fracture healing in adult *ChM-I*$^{-/-}$ mice (data not shown). It is possible that a functionally redundant factor may compensate for the lack of ChM-I activity in *ChM-*

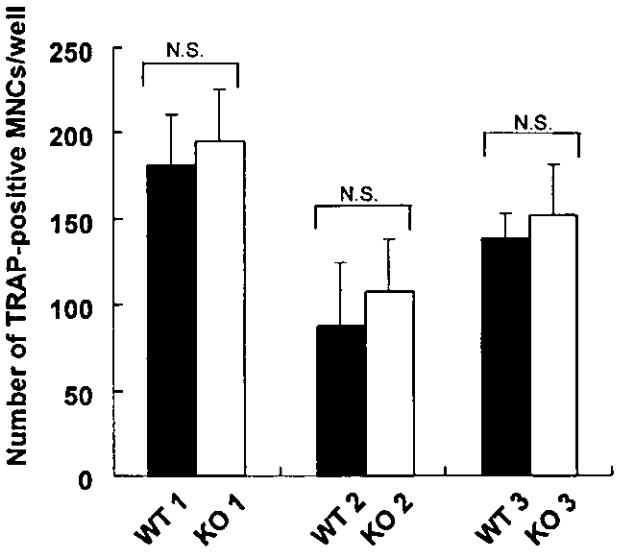

FIG. 6. In vitro osteoclastogenesis is not attached to ChM-I inactivation. Bone marrow macrophages were isolated from tibial bone marrow of 12-week-old mice and were induced to osteoclast formation by stimulation with 100 ng of M-CSF/ml and 100 ng of soluble rhRANKL/ml as described in Materials and Methods. TRAP-positive multinucleated cells (MNCs) per well were counted. Data are means ± standard deviations for four wells. WT, wild type; KO, knockout; N.S., not significant.

$I^{-/-}$ mice. While tenomodulin was once assumed to mimic ChM-I action in cartilage development, it was recently shown that its expression patterns do not overlap with that of ChM-I in cartilage (25). Moreover, tenomodulin expression was not affected by ChM-I inactivation in mice (data not shown). Thus, taken together, our study suggested the possible existence of a functionally redundant factor for ChM-I in chondrocytes.

As the only reported activity for ChM-I involved the stimulation of osteoblast proliferation and differentiation (19), which does not appear to explain the bone phenotype of the *ChM-I*$^{-/-}$ mice, the function of ChM-I in osteoclasts remains elusive. However, given the increased bone mineral density in *ChM-I*$^{-/-}$ mice, ChM-I expression in osteoblasts at low levels may regulate the expression of receptors or ligands that control the proliferation and/or differentiation of both osteoblasts and osteoclasts. In this respect, as decreased numbers of TRAP-positive mature osteoclasts were observed in *ChM-I*$^{-/-}$ mice, the possibility of the involvement of ChM-I in the RANKL-receptor activator of nuclear factor κB system of osteoclastogenesis (13, 15) is of interest and remains to be tested.

ACKNOWLEDGMENTS

We thank H. Murayama (Kureha Chemical Industry) for technical assistance with bone histology and Yasuhiro Kobayashi (Matsumoto Dental University) for helpful discussions about osteoclast generations. We thank R. Nakamura and H. Higuchi for manuscript preparation.

This work was supported by a grant-in-aid from the Japan Society for the Promotion of Science Research for the Future Program (to Y.H.) and priority areas from the Ministry of Education, Science, Sports and Culture of Japan (to S.K.).

REFERENCES

1. **Ducy, P., C. Desbois, B. Boyce, G. Pinero, B. Story, C. Dunstan, E. Smith, J. Bonadio, S. Goldstein, C. Gundberg, A. Bradley, and G. Karsenty.** 1996. Increased bone formation in osteocalcin-deficient mice. Nature **382**:448–452.
2. **Ducy, P., T. Schinke, and G. Karsenty.** 2000. The osteoblast: a sophisticated fibroblast under central surveillance. Science **289**:1501–1504.
3. **Gelb, D. E., R. N. Rosier, and J. E. Puzas.** 1990. The production of transforming growth factor-beta by chick growth plate chondrocytes in short term monolayer culture. Endocrinology **127**:1941–1947.
4. **Gerber, H. P., T. H. Vu, A. M. Ryan, J. Kowalski, Z. Werb, and N. Ferrara.** 1999. VEGF couples hypertrophic cartilage remodeling, ossification and angiogenesis during endochondral bone formation. Nat. Med. **5**:623–628.
5. **Gonzalez, A. M., M. Buscaglia, M. Ong, and A. Baird.** 1990. Distribution of basic fibroblast growth factor in the 18-day rat fetus: localization in the basement membranes of diverse tissues. J. Cell Biol. **110**:753–765.
6. **Haigh, J. J., H. P. Gerber, N. Ferrara, and E. F. Wagner.** 2000. Conditional inactivation of VEGF-A in areas of collagen2a1 expression results in embryonic lethality in the heterozygous state. Development **127**:1445–1453.
7. **Hankenson, K. D., S. D. Bain, T. R. Kyriakides, E. A. Smith, S. A. Goldstein, and P. Bornstein.** 2000. Increased marrow-derived osteoprogenitor cells and endosteal bone formation in mice lacking thrombospondin 2. J. Bone Miner. Res. **15**:851–862.
8. **Hiraki, Y., H. Inoue, K. Iyama, A. Kamizono, M. Ochiai, C. Shukunami, S. Iijima, F. Suzuki, and J. Kondo.** 1997. Identification of chondromodulin I as a novel endothelial cell growth inhibitor. Purification and its localization in the avascular zone of epiphyseal cartilage. J. Biol. Chem. **272**:32419–32426.
9. **Hiraki, Y., T. Kono, M. Sato, C. Shukunami, and J. Kondo.** 1997. Inhibition of DNA synthesis and tube morphogenesis of cultured vascular endothelial cells by chondromodulin-I. FEBS Lett. **415**:321–324.
10. **Hiraki, Y., H. Tanaka, H. Inoue, J. Kondo, A. Kamizono, and F. Suzuki.** 1991. Molecular cloning of a new class of cartilage-specific matrix, chondromodulin-I, which stimulates growth of cultured chondrocytes. Biochem. Biophys. Res. Commun. **175**:971–977.
11. **Holmbeck, K., P. Bianco, J. Caterina, S. Yamada, M. Kromer, S. A. Kuznetsov, M. Mankani, P. G. Robey, A. R. Poole, I. Pidoux, J. M. Ward, and H. Birkedal-Hansen.** 1999. MT1-MMP-deficient mice develop dwarfism, osteopenia, arthritis, and connective tissue disease due to inadequate collagen turnover. Cell **99**:81–92.
12. **Inoue, H., J. Kondo, T. Koike, C. Shukunami, and Y. Hiraki.** 1997. Identification of an autocrine chondrocyte colony-stimulating factor: chondromodulin-I stimulates the colony formation of growth plate chondrocytes in agarose culture. Biochem. Biophys. Res. Commun. **241**:395–400.
13. **Kong, Y. Y., H. Yoshida, I. Sarosi, H. L. Tan, E. Timms, C. Capparelli, S. Morony, A. J. Oliveira-dos-Santos, G. Van, A. Itie, W. Khoo, A. Wakeham, C. R. Dunstan, D. L. Lacey, T. W. Mak, W. J. Boyle, and J. M. Penninger.** 1999. OPGL is a key regulator of osteoclastogenesis, lymphocyte development and lymph-node organogenesis. Nature **397**:315–323.
14. **Kyriakides, T. R., Y. H. Zhu, L. T. Smith, S. D. Bain, Z. Yang, M. T. Lin, K. G. Danielson, R. V. Iozzo, M. LaMarca, C. E. McKinney, E. I. Ginns, and P. Bornstein.** 1998. Mice that lack thrombospondin 2 display connective tissue abnormalities that are associated with disordered collagen fibrillogenesis, an increased vascular density, and a bleeding diathesis. J. Cell Biol. **140**:419–430.
15. **Li, J., I. Sarosi, X. Q. Yan, S. Morony, C. Capparelli, H. L. Tan, S. McCabe, R. Elliott, S. Scully, G. Van, S. Kaufman, S. C. Juan, Y. Sun, J. Tarpley, L. Martin, K. Christensen, J. McCabe, P. Kostenuik, H. Hsu, F. Fletcher, C. R. Dunstan, D. L. Lacey, and W. J. Boyle.** 2000. RANK is the intrinsic hematopoietic cell surface receptor that controls osteoclastogenesis and regulation of bone mass and calcium metabolism. Proc. Natl. Acad. Sci. USA **97**:1566–1571.
16. **Li, X., N. Udagawa, K. Itoh, K. Suda, Y. Murase, T. Nishihara, T. Suda, and N. Takahashi.** 2002. p38 MAPK-mediated signals are required for inducing osteoclast differentiation but not for osteoclast function. Endocrinology **143**: 3105–3113.
17. **Malluche, H. H., D. Sherman, W. Meyer, and S. G. Massry.** 1982. A new semiautomatic method for quantitative static and dynamic bone histology. Calcif. Tissue Int. **34**:439–448.
18. **Marks, S. C., and D. C. Hermey.** 1996. The structure and development of bone, p. 3–14. *In* J. P. Bilezikian, L. G. Raise, and G. A. Rodan (ed.), Principles of bone biology. Academic Press, London, United Kingdom.
19. **Mori, Y., Y. Hiraki, C. Shukunami, S. Kakudo, M. Shiokawa, M. Kagoshima, H. Mano, Y. Hakeda, T. Kurokawa, F. Suzuki, and M. Kumegawa.** 1997. Stimulation of osteoblast proliferation by the cartilage-derived growth promoting factors chondromodulin-I and -II. FEBS Lett. **406**:310–314.
20. **Moses, M. A., J. Sudhalter, and R. Langer.** 1992. Isolation and characterization of an inhibitor of neovascularization from scapular chondrocytes. J. Cell Biol. **119**:475–482.
21. **Ogata, N., D. Chikazu, N. Kubota, Y. Terauchi, K. Tobe, Y. Azuma, T. Ohta, T. Kadowaki, K. Nakamura, and H. Kawaguchi.** 2000. Insulin receptor substrate-1 in osteoblast is indispensable for maintaining bone turnover. J. Clin. Investig. **105**:935–943.

22. **Parfitt, A. M., M. K. Drezner, F. H. Glorieux, J. A. Kanis, H. Malluche, P. J. Meunier, S. M. Ott, and R. R. Recker.** 1987. Bone histomorphometry: standardization of nomenclature, symbols, and units. Report of the ASBMR Histomorphometry Nomenclature Committee. J. Bone Miner. Res. **2**:595–610.
23. **Sekine, K., H. Ohuchi, M. Fujiwara, M. Yamasaki, T. Yoshizawa, T. Sato, N. Yagishita, D. Matsui, Y. Koga, N. Itoh, and S. Kato.** 1999. Fgf10 is essential for limb and lung formation. Nat. Genet. **21**:138–141.
24. **Shukunami, C., K. Iyama, H. Inoue, and Y. Hiraki.** 1999. Spatiotemporal pattern of the mouse chondromodulin-I gene expression and its regulatory role in vascular invasion into cartilage during endochondral bone formation. Int. J. Dev. Biol. **43**:39–49.
25. **Shukunami, C., Y. Oshima, and Y. Hiraki.** 2001. Molecular cloning of tenomodulin, a novel chondromodulin-I related gene. Biochem. Biophys. Res. Commun. **280**:1323–1327.
26. **Shukunami, C., S. Yamamoto, T. Tanabe, and Y. Hiraki.** 1999. Generation of multiple transcripts from the chicken chondromodulin-I gene and their expression during embryonic development. FEBS Lett. **456**:165–170.
27. **Suzuki, F.** 1996. Roles of cartilage matrix proteins, chondromodulin-I and -II, in endochondral bone formation: a review. Connect. Tissue Res. **35**:303–307.
28. **Takahashi, N., T. Akatsu, N. Udagawa, T. Sasaki, A. Yamaguchi, J. M. Moseley, T. J. Martin, and T. Suda.** 1988. Osteoblastic cells are involved in osteoclast formation. Endocrinology **123**:2600–2602.
29. **Takeda, S., T. Yoshizawa, Y. Nagai, H. Yamato, S. Fukumoto, K. Sekine, S. Kato, T. Matsumoto, and T. Fujita.** 1999. Stimulation of osteoclast formation by 1,25-dihydroxyvitamin D requires its binding to vitamin D receptor (VDR) in osteoblastic cells: studies using VDR knockout mice. Endocrinology **140**:1005–1008.
30. **Teitelbaum, S. L.** 2000. Bone resorption by osteoclasts. Science **289**:1504–1508.
31. **Twal, W. O., R. Vasilatos-Younken, C. V. Gay, and R. M. Leach, Jr.** 1994. Isolation and localization of basic fibroblast growth factor-immunoreactive substance in the epiphyseal growth plate. J. Bone Miner. Res. **9**:1737–1744.
32. **Uebelhart, D., E. Gineyts, M. C. Chapuy, and P. D. Delmas.** 1990. Urinary excretion of pyridinium crosslinks: a new marker of bone resorption in metabolic bone disease. Bone Miner. **8**:87–96.
33. **Vu, T. H., J. M. Shipley, G. Bergers, J. E. Berger, J. A. Helms, D. Hanahan, S. D. Shapiro, R. M. Senior, and Z. Werb.** 1998. MMP-9/gelatinase B is a key regulator of growth plate angiogenesis and apoptosis of hypertrophic chondrocytes. Cell **93**:411–422.
34. **Yagi, T., T. Tokunaga, Y. Furuta, S. Nada, M. Yoshida, T. Tsukada, Y. Saga, N. Takeda, Y. Ikawa, and S. Aizawa.** 1993. A novel ES cell line, TT2, with high germline-differentiating potency. Anal. Biochem. **214**:70–76.
35. **Yagishita, N., Y. Yamamoto, T. Yoshizawa, K. Sekine, Y. Uematsu, H. Murayama, Y. Nagai, W. Krezel, P. Chambon, T. Matsumoto, and S. Kato.** 2001. Aberrant growth plate development in VDR/RXR gamma double null mutant mice. Endocrinology **142**:5332–5341.
36. **Yoshizawa, T., Y. Handa, Y. Uematsu, S. Takeda, K. Sekine, Y. Yoshihara, T. Kawakami, K. Arioka, H. Sato, Y. Uchiyama, S. Masushige, A. Fukamizu, T. Matsumoto, and S. Kato.** 1997. Mice lacking the vitamin D receptor exhibit impaired bone formation, uterine hypoplasia and growth retardation after weaning. Nat. Genet. **16**:391–396.

Cytokines suppress adipogenesis and PPAR-γ function through the TAK1/TAB1/NIK cascade

Miyuki Suzawa*, Ichiro Takada*, Junn Yanagisawa*, Fumiaki Ohtake*, Satoko Ogawa*‡, Toshimasa Yamauchi§, Takashi Kadowaki§, Yasuhiro Takeuchi¶, Hiroshi Shibuya‡, Yukiko Gotoh*, Kunihiro Matsumoto# and Shigeaki Kato*†**

*Institute of Molecular and Cellular Biosciences, University of Tokyo, Yayoi, Bunkyo-ku, Tokyo 113-0032, Japan
†CREST, Japan Science and Technology, 4-1-8 Honcho, Kawaguchi, Saitama 332-0012, Japan
‡Division of Morphogenesis, Department of Developmental Biology, National Institute for Basic Biology, Okazaki 444-8585, Japan
§Department of Metabolic Diseases, Graduate School of Medicine, University of Tokyo, Tokyo 113-8655, Japan
¶Division of Endocrinology Department of Medicine University of Tokyo School of Medicine, Mejirodai, Bunkyo-ku, Tokyo 112-8688, Japan
#Department of Molecular Biology, Graduate School of Science, Nagoya University, Chikusa-ku, Nagoya 464-8602, Japan
**e-mail: uskato@mail.ecc.u-tokyo.ac.jp

Published online: 24 February 2003; DOI: 10.1038/ncb942

Pluripotent mesenchymal stem cells in bone marrow differentiate into adipocytes, osteoblasts and other cells[1,2]. Balanced cytodifferentiation of stem cells is essential for the formation and maintenance of bone marrow; however, the mechanisms that control this balance remain largely unknown. Whereas cytokines such as interleukin-1 (IL-1) and tumour-necrosis factor-α (TNF-α) inhibit adipogenesis[3,4], the ligand-induced transcription factor peroxisome proliferator-activated receptor-γ[5] (PPAR-γ), is a key inducer of adipogenesis. Therefore, regulatory coupling between cytokine- and PPAR-γ-mediated signals might occur during adipogenesis. Here we show that the ligand-induced transactivation function of PPAR-γ is suppressed by IL-1 and TNF-α, and that this suppression is mediated through NF-κB activated by the TAK1/TAB1/NF-κB-inducing kinase (NIK) cascade[6–9], a downstream cascade associated with IL-1 and TNF-α signalling. Unlike suppression of the PPAR-γ transactivation function by mitogen-activated protein kinase-induced growth factor signalling through phosphorylation of the A/B domain[10], NF-κB blocks PPAR-γ binding to DNA by forming a complex with PPAR-γ and its AF-1-specific co-activator PGC-2. Our results suggest that expression of IL-1 and TNF-α in bone marrow may alter the fate of pluripotent mesenchymal stem cells, directing cellular differentiation towards osteoblasts rather than adipocytes by suppressing PPAR-γ function through NF-κB activated by the TAK1/TAB1/NIK cascade.

The cytokines IL-1 and TNF-α suppress adipogenesis in bone marrow pluripotent mesenchymal stem cells *in vivo* and *in vitro*[3,4]. By contrast, PPAR-γ functions as a key inducer of adipogenesis[5]. Consistent with these reports[3,4,10], we found that adipogenesis in ST2 cells, a mesenchymal cell line derived from mouse bone marrow, could be induced, as assessed by the observation of lipid-accumulating cells and the expression of adipocyte-associated differentiation markers such as AP2 and lipoprotein lipase (LPL), by treatment with low concentrations of the PPAR-γ ligand troglitazone and that this adipogenesis could be prevented by IL-1 or TNF-α (Fig. 1a, d). Consequently, ST2 cells treated with both troglitazone and cytokines differentiated into osteoblasts expressing both alkaline phosphatase (a marker of differentiation), a protein (Fig. 1b) and mRNA (Fig. 1d)[11].

This suppressive activity of cytokines was also observed when adipogenesis was weakly induced by the synthetic glucocorticoid dexamethasone (Fig. 1a). Troglitazone induced adipogenesis in primary cultured bone marrow cells of wild-type mice, and dexamethasone induced adipogenesis less strongly; however, the potency of both ligands was considerably reduced in PPAR-$\gamma^{+/-}$ cells[5] (Fig. 1c), suggesting that PPAR-γ is crucial for adipogenesis in bone marrow stem cells. The inhibitory action of TNF-α in troglitazone-induced adipogenesis was abolished in primary cultured bone marrow cells from mice lacking both TNF receptors I and II (TNF-$RI^{-/-}II^{-/-}$; ref. 12 and Fig. 1c).

The inhibitory effects of cytokines on adipogenesis in both ST2 and primary cultured cells (Fig. 1a, c) suggested that the ligand-induced transactivation function of the PPAR-γ might be suppressed by these cytokines. To investigate this, we first examined whether cytokine treatment over short time periods (12 h) caused a reduction in both the expression and the transactivation function of PPAR-γ using a transient expression assay with PPAR-γ and retinoid-X receptor-α (RXR-α) expression vectors and a luciferase reporter plasmid containing a consensus binding site (PPAR-response element; PPRE) for the PPAR-γ/RXR-α heterodimer[13,14]. The transactivation function of troglitazone-bound PPAR-γ was suppressed markedly in ST2 cells treated with either IL-1 or TNF-α, whereas the transactivation functions of dexamethasone-bound glucocorticoid receptor (GR) and C/EBP-β were not suppressed by either cytokine (Fig. 2a). The expression of both PPAR-γ and C/EBP-β seemed to be unchanged by cytokine treatment (Fig. 1d).

Because the cell membrane receptors for IL-1 and TNF-α can activate several downstream signalling cascades[6–9], we examined the activity of several mitogen-activated protein kinase (MAPK) cascades (MKK3, MKK6, MKK7, TAK1). Overexpression of TAK1 (refs 7–9), a MAPK kinase kinase (MAP3K), mimicked cytokine activity but only in the presence of TAB1, an activator of TAK1 (ref. 9 and Fig. 2b). By contrast, we did not detect suppressed PPAR-γ function in ST2 cells in the other MAPK cascades tested (MKK3, MKK6 and MKK7; Fig. 2c). Consistent with the observation that TAK1/TAB1 is a downstream factor of TNF-α and IL-1 signalling[6–8], a kinase-negative form of TAK1 ($TAK1^{K63W}$) abrogated

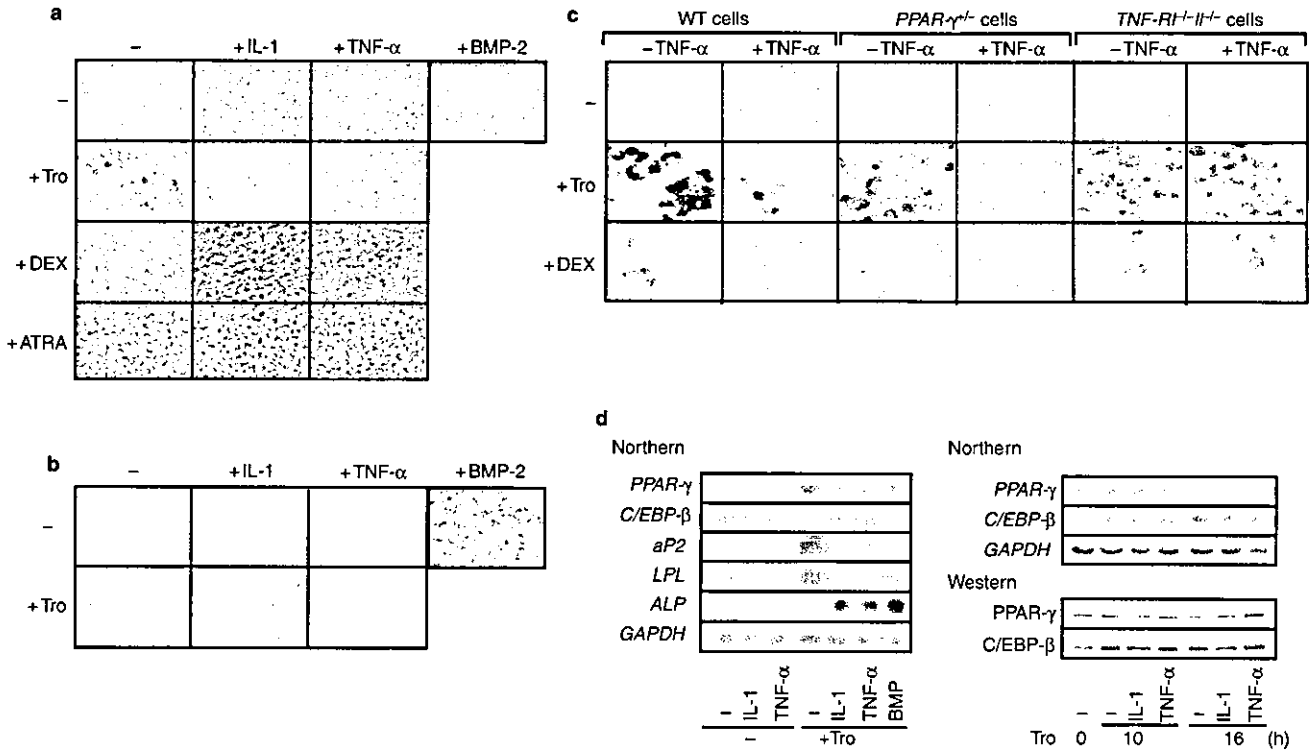

Figure 1 **IL-1 and TNF-α inhibit troglitazone-induced adipogenesis.** **a**, Inhibition of troglitazone- or dexamethasone-induced adipogenesis by IL-1 or TNF-α. Weak treatment (for 1 week) using the synthetic PPAR-γ ligand troglitazone (Tro) or dexamethasone (DEX), but not all-*trans* retinoic acid (ATRA), induces adipogenesis in ST2 cells. The presence of either IL-1 or TNF-α prevents this adipogenesis. Differentiated adipocytes were detected by the accumulation of lipid, which was stained red with Oil-Red-O. **b**, Combined treatment of cytokines and troglitazone induces osteoblastogenesis in ST2 cells. Cells were treated with cytokines and troglitazone as in **a**, and differentiated osteoblasts were stained by alkaline phosphatase. **c**, Adipocyte differentiation of wild-type, PPAR-γ$^{+/-}$ and TNF-RI$^{-/-}$II$^{-/-}$ mouse bone marrow. Primary cultured bone marrow cells derived from the corresponding mice were treated with troglitazone or dexamethasone with or without TNF-α. **d**, Differentiation of ST2 cells by troglitazone-expressed adipocyte-associated differentiation markers. Cells treated with cytokines and troglitazone for the indicated times were analysed both by northern blot for differentiation markers of adipocytes (aP2, LPL) and osteoblasts (ALP) and by western blot.

the suppressive effect of TAK1/TAB1, TNF-α and IL-1 on PPAR-γ transactivation.

We next examined NIK, a NF-κB-inducing kinase activated through phosphorylation by TAK1/TAB1 (which are activated in turn by TNF-α and IL-1)[7,8,15], for its ability to suppress PPAR-γ transactivation. Suppression mediated by NIK was clearly observed, but this suppression was abrogated when a dominant-negative form of NIK ($NIK^{629-947}$; ref. 7) was expressed (Fig. 2d). $NIK^{629-947}$ also abrogated the suppressive effects of TAK1/TAB1 and IL-1 or TNF-α treatment in ST2 cells (Fig. 2d). Consistent with these results, RNA-mediated interference (RNAi) of TAK1 and NIK expression effectively abrogated the suppressive effects of IL-1 or TNF-α in ST2 cells (Fig. 2e).

In accordance with the role of NIK in PPAR-γ transactivation, troglitazone-induced adipogenesis did not take place in stable transformants of the ST2 line expressing NIK (Fig. 2f), similar to what was observed in ST2 cells treated with TNF-α or IL-1 (Fig. 1a). By contrast, troglitazone-induced adipogenesis, even in the presence of cytokines, was observed after RNAi of TAK1 or NIK expression (Fig. 2h). As expected, adipogenesis in cell lines expressing the dominant-negative $NIK^{629-947}$ mutant was still troglitazone-sensitive; however, these NIK mutants failed to prevent the suppression of PPAR-γ transactivation through phosphorylation of Ser 112 in the A/B domain by a MAPK (ERK2) activated by the growth factor/Ras cascade (refs 10, 16 and Fig. 2g).

To determine whether the PPAR-γ transactivation function was suppressed by the TAK1/TAB1/NIK-mediated cascade or by the prevention of serine phosphorylation in the PPAR-γ A/B domain[10,16], we tested mutants in which each of the serines (Ser 8, Ser 118, Ser 274) was replaced with alanine, because analyses of the PPAR-γ deletion mutants suggested that the suppression of PPAR-γ function by cytokines was mediated by the AF-1 site in the A/B domain, and not by the AF-2 site in the carboxy terminus (data not shown). No difference in suppression was found between the wild-type and mutated receptors (Fig. 2g), suggesting that a distinct mechanism independent of serine phosphorylation in the PPAR-γ A/B domain is responsible for suppressing the PPAR-γ transactivation function. Highly similar effects of cytokines and NF-κB signal inducers on the PPAR-γ transactivation function were also seen using 293T cells, a human embryonic kidney cell line (data not shown).

To explore this molecular mechanism further, we examined the role of downstream factors of the TAK1/TAB1/NIK cascade. Overexpression of IKK-α and IKK-β, and treatment with H_2O_2 activated NF-κB[15], which then effectively suppressed the transactivation function of ligand-bound PPAR-γ in ST2 cells (Fig. 3a). In a co-immunoprecipitation assay with antibodies specific for PPAR-γ (refs 13 14), and for p50 or p65 from the NF-κB complex, we detected an association between endogenous NF-κB complex and endogenous troglitazone-bound PPAR-γ in ST2 cells, but only when cells were treated with either TNF-α or IL-1 (Fig. 3b), or when TAK1, TAB1 or NIK was overexpressed (data not shown).

Neither dexamethasone-bound GR (Fig. 3b) nor C/EBP-β (data not shown) showed this cytokine-induced association with NF-κB;

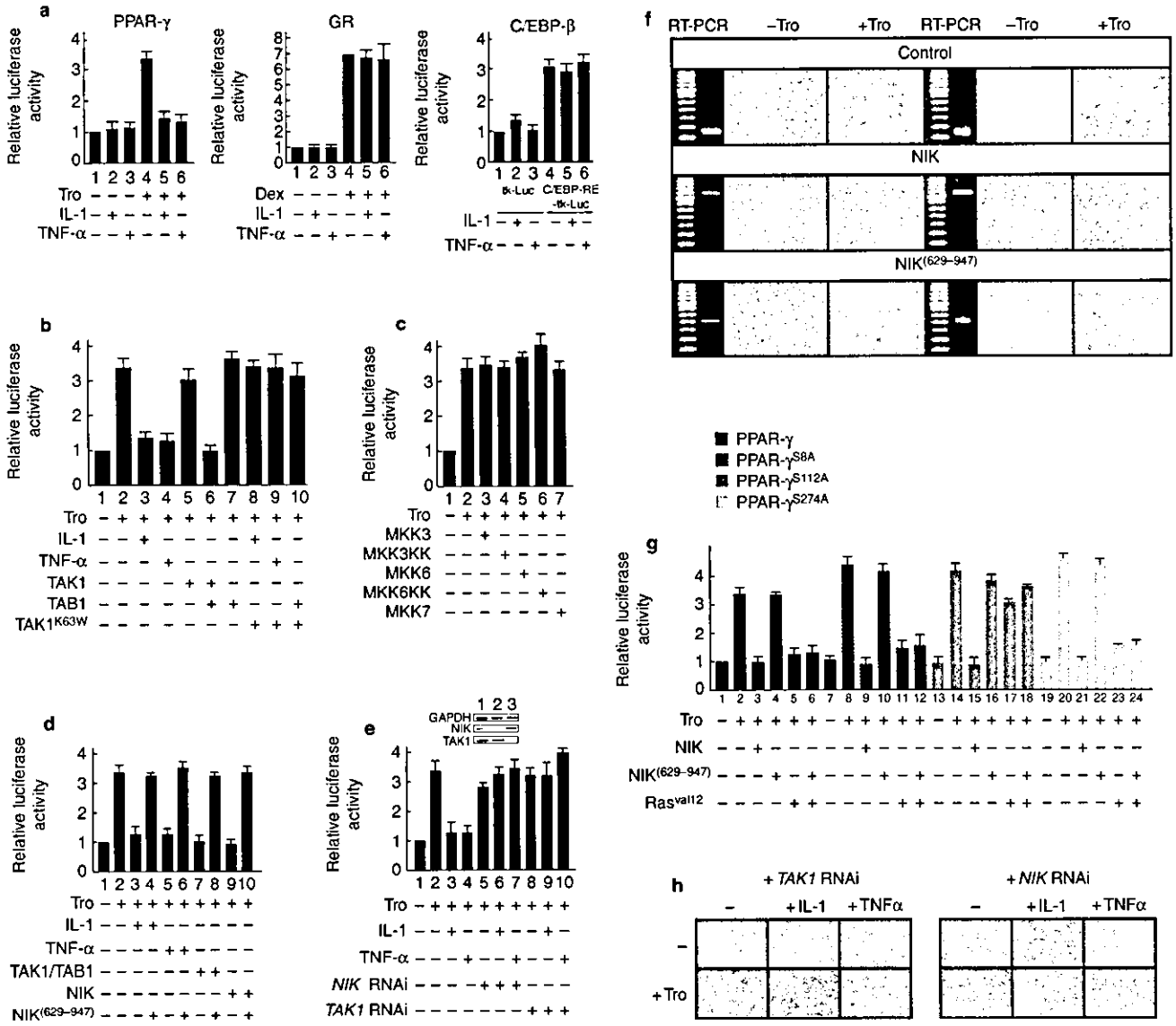

Figure 2 **TAK1/TAB1/NIK mediates suppression of PPAR-γ function.** **a**, The troglitazone-induced transactivation function of PPAR-γ is suppressed by IL-1 and TNF-α. ST2 cells were transfected with the indicated expression vectors plus mouse acyl-CoA–PPRE-tk, GRE-tk or C/EBP-RE-tk luciferase reporter plasmids and incubated for 16 h with the indicated cytokines in the absence or presence of cognate ligand. Similar results were obtained with 293T cell lines (not shown). **b**, Suppression of PPAR-γ transactivation function by TAK1/TAB1. ST2 cells were transfected with the indicated expression vectors plus the PPRE-tk luciferase reporter plasmid and incubated with the indicated cytokines for 16 h. **c**, Other MAP kinase cascades do not suppress PPAR-γ function. **d**, Suppression of PPAR-γ transactivation function by NIK. $NIK^{629-947}$ is a dominant-negative form of NIK. **e**, Suppression of PPAR-γ transactivation function by IL-1 or TNF-α is abrogated by RNAi of either NIK or TAK1. ST2 cells were co-transfected with the NIK or TAK1 RNAi vectors, and luciferase activity was assayed. Reduced expression of endogenous NIK and TAK1 was confirmed by RT–PCR (top). **f**, Inhibition of adipogenesis by NIK. ST2 stable transformants were established using the indicated NIK or $NIK^{629-947}$ expression vectors. Exogenous gene transcripts (control, 257 bp; NIK, 521 bp; $NIK^{629-947}$, 887 bp) were detected by RT–PCR. DNA molecular markers are shown in the left panels. Troglitazone-induced adipogenesis in stable transformants are shown in the right panels. **g**, The TAK1/TAB1 cascade potently inhibits phosphorylation-deficient mutants of PPAR-γ. The PPAR-γ mutants (S8A, S112A, S274A) were transfected along with NIK, $NIK^{629-947}$ or Ras^{val12} into ST2 cells. **h**, Inhibitory actions of cytokines are abolished by TAK1 or NIK RNAi. The RNAi vectors were transfected into ST2 cells and troglitazone-induced adipogenesis was examined.

thus, it seemed unlikely that the inhibited PPAR-γ transactivation function alone was responsible for the suppression of PPAR-γ function by NF-κB. We therefore tested the DNA-binding activity of endogenous PPAR-γ/RXR-α heterodimers by electrophoretic mobility shift assay (EMSA) using nuclear extracts from cytokine-treated cells. Both cytokine treatment (Fig. 3c) and overexpression of downstream factors and NF-κB (Fig. 3d) caused a considerable reduction in the ability of PPAR-γ/RXR-α heterodimers to bind to a consensus DNA-binding site (acyl-CoA-PPRE) in ST2 cells and 293T cells (data not shown), suggesting that PPAR-γ/RXR-α associates directly with NF-κB in cell nuclei. By contrast, cytokine treatment did not clearly inhibit DNA binding by GR in either cell line (data not shown).

We examined this association further with *in vitro* translated proteins and glutathione *S*-transferase (GST) fusion proteins (Fig. 3e, f). DNA binding by PPAR-γ/RXR-α was inhibited both by

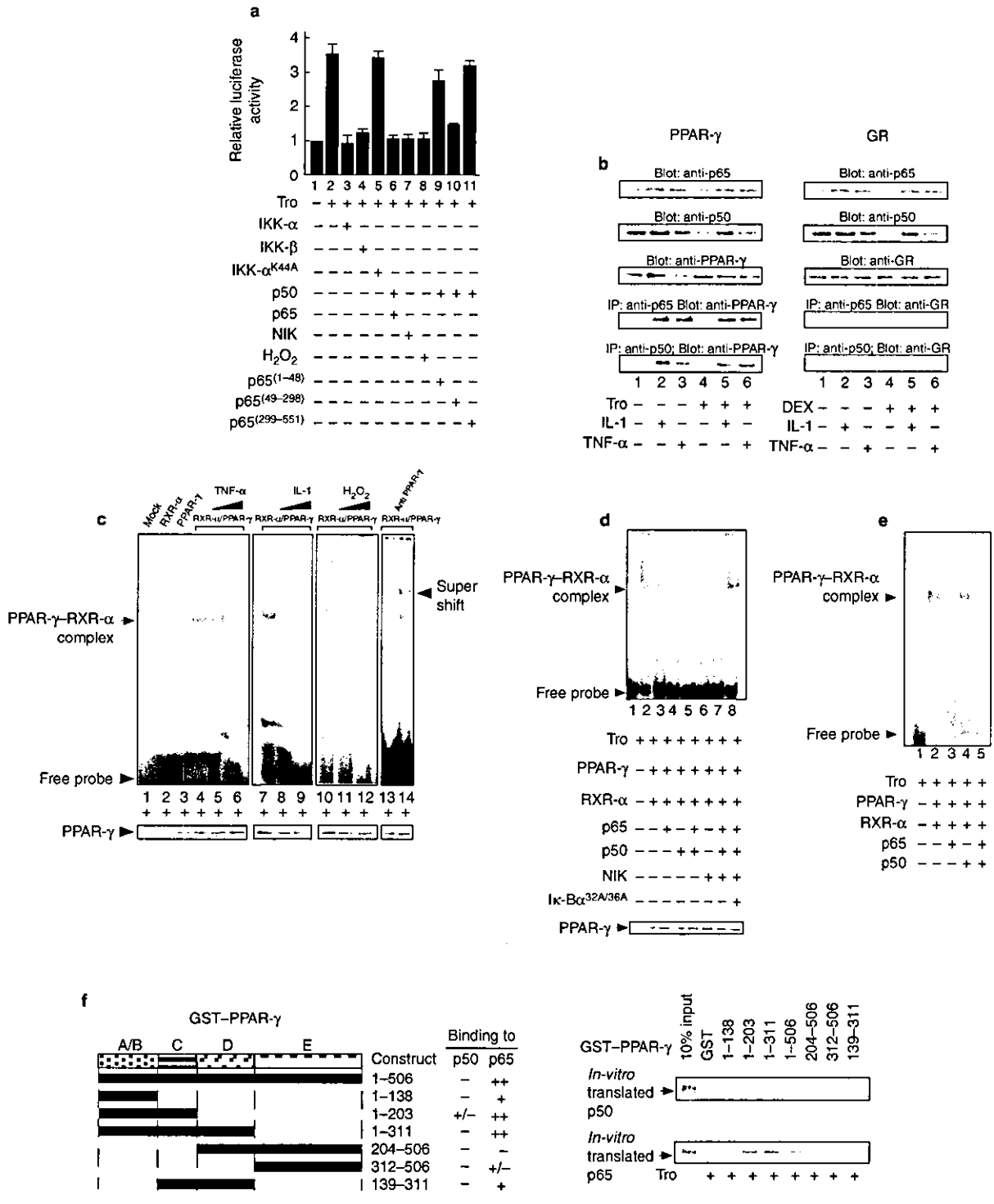

Figure 3 **NF-κB prevents DNA binding by the PPAR-γ/RXR-α heterodimer.** **a**, PPAR-γ function is suppressed by NIK-activated NF-κB. Vectors expressing the indicated signal inducers, which function downstream of NIK, were transfected into ST2 cell lines. **b**, NF-κB associates with PPAR-γ in the nucleus. Endogenous ligand-bound PPAR-γ and endogenous NF-κB complex were co-immunoprecipitated with antibodies against p65 or p50 (left) only when the cells were treated with cytokines. Cytokine treatment induced the association of PPAR-γ with the NF-κB complex in the nucleus. No endogenous GR was co-immunoprecipitated with the p65 or p50 antibodies (right). **c**, NF-κB-mediated inhibition of DNA binding by PPAR-γ is activated by cytokine signalling or H_2O_2 treatment. EMSA was done with nuclear extracts from ST2 cells transfected with the indicated expression vectors and treated with TNF-α (0.1 or 1 ng ml^{-1}), IL-1 (1.0 or 10 ng ml^{-1}) or H_2O_2 (0.1 or 1 mM). Expression of PPAR-γ was monitored by western blot using an antibody against PPAR-γ. A super-shift in the DNA-bound PPAR-γ/RXR-α heterodimer (lane 14) is indicated. **d**, Suppression of PPAR-γ DNA binding by NF-κB. IκBα$^{32A/36A}$ is a constitutive degradation-resistant mutant that inhibits NF-κB signalling[9]. **e**, Suppression of PPAR-γ DNA binding by NF-κB *in vitro*. *In vitro* translated p50, p65, PPAR-γ and RXR-α were used for EMSA as described in **c**. **f**, The NF-κB-interacting domain of PPAR-γ. GST fusion proteins of PPAR-γ deletion mutants were expressed in bacteria and used in GST pull-down assays with *in vitro* translated NF-κB.

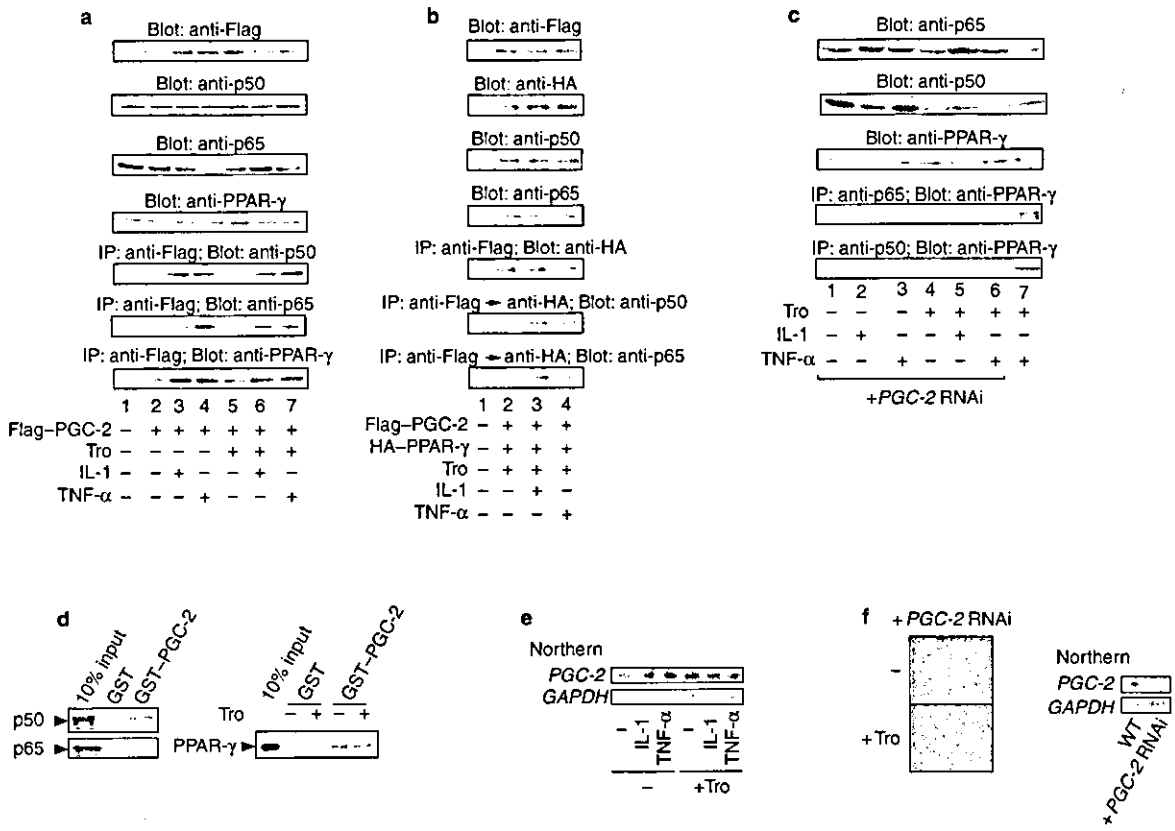

Figure 4 **Cytokine-induced association of PPAR-γ, NF-κB and PGC-2. a**, NF-κB associates with PGC-2. Exogenous Flag–PGC-2 and endogenous NF-κB complex were co-immunoprecipitated with antibodies against p65 or p50. **b**, Cytokine-dependent association of NF-κB with PGC-2 and PPAR-γ. ST2 cells transfected with Flag–PGC-2 and HA–PPAR-γ expression vectors were subjected to immunoprecipitation with antibodies against Flag, followed by antibodies against HA. NF-κB was co-immunoprecipitated with PGC-2 and PPAR-γ only when the cells were treated with cytokines. **c**, PGC-2 RNAi attenuates the cytokine-induced association of PPAR-γ/RXR with NF-κB. ST2 cells transfected with the PGC-2 RNAi vector were subjected to immunoprecipitation with antibodies against p65 or p50. **d**, PGC-2 interacts with NF-κB *in vitro*. Interaction of PGC-2 with either NF-κB (p50, p65) or PPAR-γ was examined by a GST pull-down assay. **e**, Cytokines and PPAR-γ ligand do not regulate PGC-2 expression in ST2 cells. Cells were treated with cytokines and troglitazone for 1 week and analysed by northern blot. **f**, PGC-2 RNAi attenuates troglitazone-induced adipogenesis in ST2 cells. Cells were transfected with PGC-2 RNAi vectors and treated with troglitazone to induce adipogenesis. Reduced expression of endogenous PGC-2 was confirmed by northern blot.

NF-κB and by p65 alone (Fig. 3e). The DNA-binding C domain of PPAR-γ was identified as a p65-interacting region (Fig. 3f), and a Rel-homology region (residues 49–298) in p65 (ref. 17) seemed to interact directly with PPAR-γ (data not shown) by GST pull-down assay. Accordingly, a $p65^{49-298}$ deletion mutant retained its function as an inhibitor of PPAR-γ (Fig. 3a), despite lacking the core DNA-binding domain[17].

We studied the molecular mechanism of the recruitment of NF-κB to PPAR-γ in bone marrow cell nuclei by examining potential PPAR-γ co-activators and co-repressors. Endogenous NF-κB did not associate directly with p160 family proteins (SRC-1/TIF2/AIB1)[13,14], DRIP205/TRAP220 (ref. 13) or NCoR/SMRT (data not shown), but it did associate directly with PGC-2, a PPAR-γ AF-1-specific co-activator (ref. 18 and Fig. 4a). This cytokine-induced interaction was detected when the complex was immunoprecipitated sequentially with PGC-2 and then PPAR-γ (Fig. 4b, c), suggesting that NF-κB associates with PGC-2-bound PPAR-γ. PGC-2 also interacted directly with NF-κB and PPAR-γ in the GST pull-down assay (Fig. 4d). Note that expression of the PGC-2 gene was unchanged by any treatment (Fig. 4e) and that the troglitazone-induced adipogenesis was attenuated by RNAi of PGC-2 expression (Fig. 4f). These findings suggest that NF-κB translocating into the nuclei is preferentially recruited to PPAR-γ through direct association with PGC-2, forming a complex that inhibits DNA binding by PPAR-γ.

We next tested whether the suppression of PPAR-γ function by the TAK1/TAB1/NIK cascade reflects physiological events in the transcriptional regulation of PPAR-γ target genes[5,19]. Induction of the early response gene encoding c-Cbl-associated protein (CAP) in response to the PPAR-γ ligand[19] was blocked by treatment with TNF-α or IL-1 (Fig. 5a). Consistent with these results, chromatin immunoprecipitation (ChIP) analysis[19,20] showed that troglitazone-induced histone (H4) acetylation around PPRE in the CAP gene promoter by PPAR-γ was abrogated by cytokine treatment (Fig. 5b). In addition, cytokine treatment blocked DNA binding by PPAR-γ, but not by GR and C/EBP-β (ref. 21 and Fig. 5b, bottom). Thus, these findings indicate that TNF-α and IL-1 signalling suppress the expression of endogenous target genes for PPAR-γ through NF-κB-mediated blocking of the binding of PPRE by endogenous PPAR-γ/RXR-α heterodimers, thereby exerting an inhibitory effect on adipogenesis.

Among the cytokines expressed in bone marrow, TNF-α and IL-1, which act as principal inducers of osteoclastogenesis from progenitor cells of monocyte/macrophage lineage[22], are known to inhibit adipogenesis[3,4], directing bone marrow stem cells towards osteoblastogenesis and the formation of trabecular bone[2]. But the molecular mechanisms by which these cytokines inhibit adipogenesis remain unclear. Given the wide acceptance of PPAR-γ as a principal inducer of adipogenesis[5], and the development of numerous

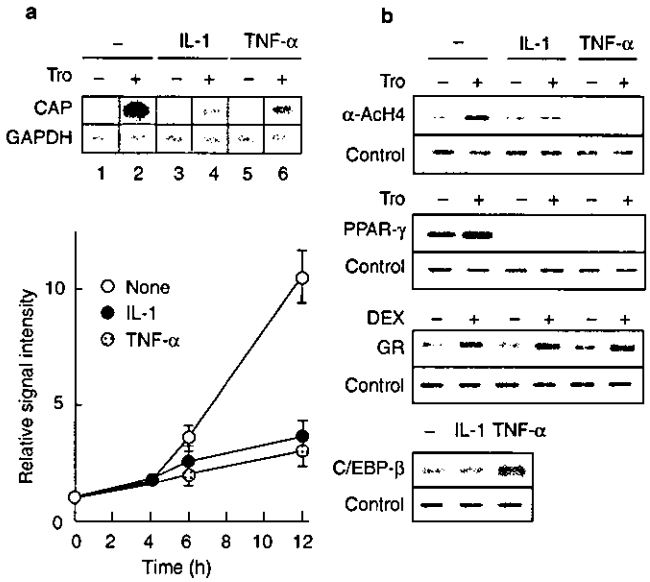

Figure 5 **Blocking PPAR-γ function inhibits adipogenesis through the NIK cascade. a**, Treatment with TNF-α or IL-1 prevents troglitazone-induced expression of an early response target gene of PPAR-γ. ST2 cells were treated with cytokines for the indicated times and total RNA was analysed by northern blot for the gene encoding CAP. Representative results at 8 h of treatment are shown at the top. Densitometric analysis of CAP expression is shown below. **b**, Cytokine treatment inhibits troglitazone-induced histone acetylation and PPAR-γ DNA binding in the promoter of CAP. A ChIP assay[20] was done on cells treated with cytokines for 12 h. The PPRE-containing region (–1110 to –801) in the CAP promoter[19], the GRE-containing region (–528 to –110) in the PEPCK promoter or the C/EBP-RE-containing region (–361 to –73) in the PPAR-γ2 promoter[21] were amplified by PCR. Note that TNF-α and IL-1 inhibit the troglitazone-induced acetylation of histone H4 and the binding of PPAR-γ to the CAP promoter, clearly indicating that these cytokines inhibit the function of troglitazone-bound PPAR-γ on the PPRE. By contrast, no inhibition of the binding of GR or C/EBP-β to the target gene promoters was observed on cytokine treatment.

synthetic PPAR-γ ligands for the treatment of diabetes and the modulation of adipogenesis[23], we chose to investigate the effect of cytokines on PPAR-γ function.

Our results show that, of the signalling cascades downstream of TNF-α and IL-1, the TAK1/TAB1/NIK cascade suppresses PPAR-γ function by preventing PPAR-γ binding to DNA through an association with NF-κB that is coupled to the suppression of AF-1 function; this suggests that these cytokines reduce PPAR-γ function in pluripotent bone marrow stem cells, although the other signalling cascades[24] that activate NF-κB may also contribute to the PPAR-γ suppression. Together with studies showing that the activation of PPAR-γ signalling in the progenitor cells of lineage monocyte/macrophage inhibits osteoclastogenesis by suppressing NF-κB function[25], it is likely that the suppression of PPAR-γ function increases the sensitivity of stem cells to other cytodifferentiation factors, thereby inducing the development of cell types other than adipocytes, such as osteoblasts and osteoclasts[1,2,25].

In the nucleus, translocated NF-κB seems to interact directly both with the DNA-binding domain of PPAR-γ and with PGC-2 bound to AF-1 in the A/B domain of PPAR-γ, and the resultant complex blocks the binding of PPAR-γ/RXR-α heterodimers to target gene promoters. Because the functions of PPAR-γ AF-1 and PGC-2 have important roles in fat cell differentiation, this interaction with NF-κB may also interfere with their adipogenic functions. Although NF-κB is reported to associate with many other nuclear receptors, NF-κB seems to be recruited preferentially to PPAR-γ, at least in bone marrow stem cells, by its interaction with PGC-2, because the physical interaction of PGC-2 with PPAR-γ is highly selective among nuclear receptors[18]. Previous reports have shown that NF-κB function is inhibited by PPAR-γ ligands, including troglitazone, which act as anti-inflammatory agents[26,27]. It therefore seems that complexes formed by ligand-bound PPAR-γ, NF-κB and unknown factors lead to mutual inactivation of both classes of transcription regulatory factor, probably by suppressing their functions.

In this respect, it would be interesting to examine whether nuclear receptor co-repressors (for example, NCoR and SMRT) are included in this complex, because findings in NcoR knockout mice[28] have raised the possibility that such co-repressors are recruited to both ligand-bound PPAR-γ and to unliganded PPAR-γ and suppress transcription by associating with histone deacetylases[29], resulting in chromatin in an inactive state. The identification of other components in the PPAR-γ–NF-κB complexes would be of interest, because it would increase our understanding of coupled transcriptional regulation mediated by distinct classes of regulatory factor located in the same complex. □

Methods

Plasmid construction

We inserted full-length PPAR-γ cDNA or Flag–PGC-2 cDNA into pcDNA3 (Invitrogen, Carlsbad, CA)[13,18]. Full-length p50 and the p65 mutant cDNAs were inserted into pcDNA3 vectors (Invitrogen). TAK1, TAK1^{K63W}, TAB1, NIK, NIK$^{629-947}$, MKK3, MKK3KK, MKK6, MKK6KK, MKK7, IKK-α, IKK-β, IKK-α^{K44A}, IκB-α and IκB-α$^{32A/36A}$ have been described[2–9]. A PPRE (3 × acyl-CoA-PPRE), a glucocorticoid response element (GRE), a C/EBP response element (C/EBP-RE)[21] and an 8 × GAL4-binding element (17M8) were inserted into the luciferase pGL3-basic vector (Promega, Madison, WI) as reporter plasmids. The bacterial GST fusion protein expression vector for GST-bound fragments of PPAR (residues 1–506, 1–138, 1–203, 1–311, 204–506, 312–506 and 139–311) and PGC-2 (refs 13, 18) were inserted into the pGEX 4T-1 vector (Amersham Pharmacia, Piscataway, NJ). We generated RNAi constructs (NIK, +34 to +53; TAK1, +84 to +103; PGC-2, –14 +6) in an mU6-pro vector[10].

Cell culture

ST2 stromal cells derived from mouse bone marrow were cultured in α-MEM medium containing 10% fetal bovine serum (FBS) and treated with TNF-α (1 ng ml^{-1}), IL-1 (10 ng ml^{-1}), H_2O_2 (1 mM), troglitazone (1 μM), dexamethasone (0.1 μM), all-*trans* retinoic acid (10 nM) or combinations thereof. After 7 d, lipid accumulation was assessed by staining with Oil-Red-O to detect adipocytes. We derived NIK and NIK$^{629-947}$ stable transformants by transfecting the ST2 cell line. Primary cultured bone marrow cells were obtained from femoral and tibia cells of wild-type, PPAR-γ$^{+/-}$ or TNF-RI$^{-/-}$II$^{-/-}$ mice[5,12] by flushing with α-MEM, and contaminated red blood cells were haemolysed in 0.017 M Tris-HCl (pH 7.5) buffer containing 0.8% ammonium chloride. We rinsed cell suspensions in PBS twice and cultured them in α-MEM with 10% FBS at 37 °C.

Transfection and luciferase assay

Cells at 40–50% confluence were transfected in 12-well petri dishes by Lipofectamine regent (Gibco-BRL, Grand Island, NY). The total amount of DNA was adjusted to 1.0 μg by adding empty vector. We determined luciferase activity by using the Luciferase Assay System (Promega, Madison, WI). As a reference plasmid to normalize transfection efficiency, 25 ng of pRL-CMV plasmid (Promega) was co-transfected in all experiments[14,16].

Co-immunoprecipitation and western blotting

The transfected ST2 cells were washed twice in ice-cold PBS, collected, resuspended in 1 ml of ice-cold lysis buffer (10 mM Tris-HCl (pH 7.5), 1% Nonidet P-40, 0.15 M NaCl and 1 mM EDTA) and incubated for 30 min on ice. After centrifugation, supernatants were used as whole-cell extracts for immunoprecipitation with antibodies against either p50 or p65 (Santa Cruz Biotechnology, Santa Cruz, CA), followed by western blotting with antibodies specific for human PPAR-γ (H-100; Santa Cruz Biotechnology, Santa Cruz, CA)[14], GR (ABR, Golden, CO), Flag (anti-Flag monoclonal antibody; Sigma, St Louis, MI) or haemagglutinin A (HA; MBL, Nagoya, Japan).

Alkaline phosphatase staining

For histochemical staining of alkaline phosphatase[11], cells were fixed for 10 min with 3.7% formaldehyde at room temperature. After washing the cells in PBS, we incubated them for 20 min at room temperature with a mixture of 0.1 mg ml^{-1} naphthol AS-MX phosphate (Sigma), 0.5% *N,N*-dimethylformamide, 2 mM $MgCl_2$ and 0.6 mg ml^{-1} of fast blue BB salt (Sigma, St Louis, MI) in 0.1 M Tris-HCl (pH 8.5).

GST pull-down assay

Human PPAR-γ, PGC-2 and the deletion mutants were expressed as GST fusion proteins in *Escherichia coli* as described[13] and bound to glutathione-conjugated Sepharose 4B beads (Amersham Pharmacia). *In vitro* translated NF-κB proteins were incubated with the beads in NET-N buffer (0.5% Nonidet P-40, 20 mM Tris-HCl (pH 7.5), 200 mM NaCl, 1 mM EDTA) containing 1 mM phenyl methylsulphonyl fluoride. We separated the bound proteins by 7.5% SDS–PAGE, lightly stained them with Coomasie brilliant blue to verify equal amounts of fusion proteins and then visualized them by autoradiography.

EMSA

Nuclear extracts were prepared from transfected ST2 cells 30 min after cytokine treatment. Binding

reactions using acyl-CoA-PPRE as a DNA probe were done on ice for 30 min in binding buffer (10 mM HEPES (pH 7.9), 100 mM KCl, 7.5% glycerol, 1 mM dithiothreitol and 0.1% Nonidet P-40), 2 μg poly (dI-dC) and 10 μg of bovine serum albumin in a final volume of 25 μl. An antibody against PPAR-γ2 (ABR) was added to detect a supershift. Labelled PPRE DNA fragments were added to the binding mixtures, and further incubated for 20 min at room temperature. Whole reaction mixtures (25 μl) were loaded onto 5.0% polyacrylamide gels in Tris-acetate-EDTA buffer and separated by electrophoresis at 4 °C. We dried gels on filter paper and exposed them to X-ray film[13].

Northern blot analysis

Total cellular RNA was isolated from ST2 cells by Isogen (Wako, Osaka, Japan), and 20 μg of RNA was used for northern blot analysis with cDNAs for CAP, PPAR-γ, C/EBP-β, aP2, LPL, alkaline phosphatase, PGC-2 and glyceraldehyde-3-phosphate dehydrogenase (GAPDH) used as probes[13,14].

ChIP assay

We cultured ST2 cells for 2 d in the presence or absence of troglitazone or dexamethasone with or without cytokines and used the ChIP Assay Kit (Upstate Biotechnology, Lake Placid, NY) with an antibody[14] against acetylated histone H4, the H-100 antibody against human PPAR-γ, an antibody against GR antibody or antibodies against C/EBP-β (Santa Cruz Biotechnology, Santa Cruz, CA). For amplification by polymerase chain reaction (PCR), we used the primer pair 5′-GTCAACTTGACACAGGCTAA-3′ (−1110 to 1091) and 5′-TTAGACTTCCACAACGCTGCT-3′ (−819 to − 801) in the CAP gene promoter region for PPRE[36], 5′-GTAACACACCCCAGCTAACT-3′ (−528 to −509) and 5′-ATCATAGCCATGGTCAGCAC-3′ (−129 to −110) in the phosphoenolpyruvate carboxykinase (PEPCK) gene promoter region for GRE and 5′-GCCACTGGTGTG-TATTTTAC-3′ (−361 to −342) and 5′-CAAATATTTGGGAGAGGTGGG-3′ (−93 to −73) in the PPAR-γ2 gene promoter region for C/EBP-RE[21]. Optimal PCR conditions for semi-quantitative measurement were 24 cycles of 30 s at 96 °C, 15 s at 58 °C, and 1 min at 72 °C. PCR products were visualized on 2% agarose/Tris-Acetate-EDTA (TAE) gels[36].

RECEIVED 2 APRIL 2002; REVISED 9 NOVEMBER 2002; ACCEPTED 18 NOVEMBER 2003; PUBLISHED 24 FEBRUARY 2003.

1. Gimble, J. M. *et al.* Bone morphogenetic proteins inhibit adipocyte differentiation by bone marrow stromal cells. *J. Cell. Biochem.* 58, 393–402 (1995).
2. Ducy, P., Schinke, T. & Karsenty, G. The osteoblast: a sophisticated fibroblast under central surveillance. *Science* 289, 1501–1504 (2000).
3. Ron, D., Brasier, A. R., McGehee, R. J. & Habener, J. F. Tumor necrosis factor-induced reversal of adipocytic phenotype of 3T3-L1 cells is preceded by a loss of nuclear CCAAT/enhancer binding protein (C/EBP). *J. Clin. Invest.* 89, 223–233 (1992).
4. Torti, F. M., Torti, S. V., Larrick, J. W. & Ringold, G. M. Modulation of adipocyte differentiation by tumor necrosis factor and transforming growth factor β. *J. Cell. Biol.* 108, 1105–1113 (1989).
5. Kubota, N. *et al.* PPARγ mediates high-fat diet-induced adipocyte hypertrophy and insulin resistance. *Mol. Cell* 4, 597–609 (1999).
6. Takaesu, G. *et al.* TAB2, a novel adaptor protein, mediates activation of TAK1 MAPKKK by linking TAK1 to TRAF6 in the IL-1 signal transduction pathway. *Mol. Cell* 5, 649–658 (2000).
7. Ninomiya-Tsuji, J. *et al.* The kinase TAK1 can activate the NIK–IκB as well as the MAP kinase cascade in the IL-1 signalling pathway. *Nature* 398, 252–256 (1999).
8. Shirakabe, K. *et al.* TAK1 mediates the ceramide signalling to stress-activated protein kinase/c-Jun N-terminal kinase. *J. Biol. Chem.* 272, 8141–8144 (1997).
9. Shibuya, H. *et al.* TAB1: an activator of the TAK1 MAPKKK in TGF-β signal transduction. *Science* 272, 1179–1182 (1996).
10. Hu, E., Kim, J. B., Sarraf, P. & Spiegelman, B. M. Inhibition of adipogenesis through MAP kinase-mediated phosphorylation of PPARγ. *Science* 274, 2100–2103 (1996).
11. Yamaguchi, A., Komori, T., Suda, Regulation of osteoblast differentiation mediated by bone morphogenetic proteins, hedgehogs, and Cbfa1. Endocr. Rev. 21, 393–411 (2000).
12. Peschon, J. J. et al. TNF receptor-deficient mice reveal divergent roles for p55 and p75 in several models of inflammation. J. Immunol. 160, 943–952 (1998).
13. Kodera, Y. *et al.* Ligand type-specific interactions of peroxisome proliferator-activated receptor γ with transcriptional coactivators. *J. Biol. Chem.* 275, 33201–33204 (2000).
14. Yanagisawa, J. *et al.* Convergence of transforming growth factor-β and vitamin D signalling pathways on SMAD transcriptional coactivators. *Science* 283, 1317–1321 (1999).
15. Woronicz, J. D., Gao, X., Cao, Z., Rothe, M. & Goeddel, D. V. IkB kinase-b: NF-kB activation and complex formation with IkB kinase-a and NIK. Science 278, 866–869 (1997).
16. Kato, S. et al. Activation of the estrogen receptor through phosphorylation by mitogen-activated protein kinase. Science 270, 1491–1494 (1995).
17. Chen, F. E., Huang, D. B., Chen Y. O. & Ghosh, G. Crystal structure of p50/p65 heterodimer of transcription factor NF-kB bound to DNA. Nature 391, 410–413 (1998).
18. Castillo, G. et al. An adipogenic cofactor bound by the differentiation domain of PPARg. EMBO J. 13, 3676–3687 (1999).
19. Baumann, C. A., Chokshi, N., Saltiel, A. R. & Ribon, V. Cloning and characterization of a functional peroxisome proliferator activator receptor-gamma-responsive element in the promoter of the CAP gene. *J. Biol. Chem.* 275, 9131–9135 (2000).
20. Chen, H., Lin, R. J., Xie, W., Wilpitz, D. & Evans, R. M. Regulation of hormone-induced histone hyperacetylation and gene activation via acetylation of an acetylase. *Cell* 98, 675–86 (1999).
21. Zhu, Y. et al. Structural organization of mouse peroxisome proliferator-activated receptor g (mPPARg) gene: alternative promoter use and different splicing yield two mPPAR g isoforms. Proc. Natl Acad. Sci. USA 17, 7921–7925 (1995).
22. Teitelbaum, S. L. Bone resorption by osteoclasts. *Science* 289, 1504–1508 (2000).
23. Kersten, S., Desvergne, B. & Wahli, W. Roles of PPARs in health and disease. *Nature* 405, 421–424 (2000).
24. Wajant, H., Henkler, F. & Scheurich, P. The TNF-receptor-associated factor family: scaffold molecules for cytokine receptors, kinases and their regulators. Cell Signal 13, 389–400 (2001).
25. Mbalaviele, G. et al. Activation of peroxisome proliferator-activated receptor-g pathway inhibits osteoclast differentiation. J. Biol. Chem. 275, 14388–14393 (2000).
26. Ricote, M., Li, A. C., Willson, T. M., Kelly, C. J. & Glass, C. K. The peroxisome proliferator-activated receptor-g is a negative regulator of macrophage activation. Nature 391, 79–82 (1998).
27. Rossi, A. *et al.* Anti-inflammatory cyclopentenone prostaglandins are direct inhibitors of IκB kinase. *Nature* 403, 103–108 (2000).
28. Jepsen, K. *et al.* Combinatorial roles of the nuclear receptor corepressor in transcription and development. *Cell* 102, 753–763 (2000).
29. Glass, C. K. & Rosenfeld, M. G. The coregulator exchange in transcriptional functions of nuclear receptors. *Genes Dev.* 14, 121–141 (2000).
30. Yu, J. Y., DeRuiter, S. L. & Turner, D. L. RNA interference by expression of short-interfering RNAs and hairpin RNAs in mammalian cells. Proc. Natl Acad. Sci. USA 99, 6047–6052 (2002).

ACKNOWLEDGEMENTS

We thank S. Tanaka for discussions; R. Nakamura and H. Higuchi for manuscript preparation; Sankyo Pharmaceuticals for troglitazone; P. Chambon for the mouse RXR-α cDNA; and D. Turner for the RNAi vector. This work was supported in part by a Grant-in-Aid for Priority Areas from the Ministry of Education, Science, Sports and Culture of Japan (to S.K.).

Correspondence and requests for materials should be addressed to S.K.

COMPETING FINANCIAL INTERESTS

The authors declare that they have no competing financial interests.

Cell, Vol. 113, 905–917, June 27, 2003, Copyright ©2003 by Cell Press

The Chromatin-Remodeling Complex WINAC Targets a Nuclear Receptor to Promoters and Is Impaired in Williams Syndrome

Hirochika Kitagawa,[1,2] Ryoji Fujiki,[1] Kimihiro Yoshimura,[1] Yoshihiro Mezaki,[1] Yoshikatsu Uematsu,[1] Daisuke Matsui,[1] Satoko Ogawa,[1] Kiyoe Unno,[1,3] Mataichi Okubo,[3] Akifumi Tokita,[3] Takeya Nakagawa,[4] Takashi Ito,[4] Yukio Ishimi,[5] Hiromichi Nagasawa,[6] Toshio Matsumoto,[2] Junn Yanagisawa,[1,7] and Shigeaki Kato[1,7,*]

[1]Institute of Molecular and Cellular Biosciences
University of Tokyo
1-1-1 Yayoi
Bunkyo-ku
Tokyo 113-0032
Japan

[2]First Department of Internal Medicine
University of Tokushima School of Medicine
3-18-15 Kuramoto-cho
Tokushima 770-8503
Japan

[3]Department of Pediatrics
Juntendo University School of Medicine
3-1-3 Hongo
Bunkyo-ku
Tokyo 113-8431
Japan

[4]Department of Biochemistry
Nagasaki University School of Medicine
1-12-4 Sakamoto
Nagasaki 852-8523
Japan

[5]Mitsubishi Kagaku Institute of Life Sciences
11 Minamiooya
Machida-shi
Tokyo 194-8511
Japan

[6]Department of Applied Biological Chemistry
Graduate School of Agricultural and Life Sciences
University of Tokyo
1-1-1 Yayoi
Bunkyo-ku
Tokyo 113-0032
Japan

[7]SORST
Japan Science and Technology
4-1-8 Honcho
Kawaguchi
Saitama 332-0012
Japan

Summary

We identified a human multiprotein complex (WINAC) that directly interacts with the vitamin D receptor (VDR) through the Williams syndrome transcription factor (WSTF). WINAC has ATP-dependent chromatin-remodeling activity and contains both SWI/SNF components and DNA replication-related factors. The latter might explain a WINAC requirement for normal S phase progression. WINAC mediates the recruitment of unliganded VDR to VDR target sites in promoters, while subsequent binding of coregulators requires ligand binding. This recruitment order exemplifies that an interaction of a sequence-specific regulator with a chromatin-remodeling complex can organize nucleosomal arrays at specific local sites in order to make promoters accessible for coregulators. Furthermore, overexpression of WSTF could restore the impaired recruitment of VDR to vitamin D regulated promoters in fibroblasts from Williams syndrome patients. This suggests that WINAC dysfunction contributes to Williams syndrome, which could therefore be considered, at least in part, a chromatin-remodeling factor disease.

*Corresponding author: uskato@mail.ecc.u-tokyo.ac.jp

Introduction

Lipophilic ligands, such as fat-soluble vitamins A/D and thyroid/steroid hormones, exert their actions through transcriptional control of particular sets of target genes by direct binding and consequent activation of their cognate nuclear receptors (NRs) (Mangelsdorf et al., 1995). NRs form a superfamily and act as ligand-inducible regulators. From their functional and structural similarities, NR proteins are divided into five functional domains, designated A to E. The ligand binding domain (LBD) is located in the C-terminal E domain. The most conserved domain, C, is located in the NR center and serves as the DNA binding domain to specifically recognize and directly bind to their cognate ligand response elements in the target promoters. The LBD also harbors ligand-inducible transactivation function (AF-2). Upon ligand binding, NRs control transcription through ligand-dependent associations with a number of coregulators and coregulator complexes (Glass and Rosenfeld, 2000).

At transcriptional initiation sites in promoters, distinct classes of multiprotein complexes are thought to be indispensable for controlling transcription of sequence-specific regulators (Emerson, 2002; Narlikar et al., 2002). These complexes modify the chromatin configuration in a highly regulated manner, like nucleosome rearrangement, and bridge the functions between regulators and basal transcription factors, along with RNA polymerase II. Two major classes of chromatin-modifying complexes have been well characterized and their anchoring to the promoters presumably requires enzyme-catalyzed modifications of histone tails in chromatin (Hassan et al., 2002). One class contains several discrete subfamilies of transcription coregulatory complexes with either histone acetylase (HAT) or histone deacetylase (HDAC) activities to covalently modify histones through acetylation. In NR

ligand-induced transactivation processes, the complexes containing HDAC first act to corepress transactivation of unliganded NRs, while upon ligand binding, two HAT complexes, p160/CBP and TRRAP/GCN5, coactivate the NR function, like the other non-HAT DRIP/TRAP/SMCC coactivator complexes (Onate et al., 1995; Kamei et al., 1996; Rachez et al., 1998; Gu et al., 1999; Yanagisawa et al., 2002).

Another class of complexes uses ATP hydrolysis to rearrange nucleosomal arrays in a noncovalent manner and render chromosomal DNA accessible for sequence-specific regulators (Narlikar et al., 2002). These ATP-dependent chromatin-remodeling complexes act on transcription, DNA repair, and DNA replication and have been classified into subfamilies based on the major catalytic components with ATPase activity, SWI2/SNF2, ISWI, and Mi-2 (Fyodorov and Kadonaga, 2001; Yasui et al., 2002). These ATPases are highly conserved from yeast to humans and each forms a functionally similar, but distinct complex with a combination of specific components. However, the roles of most of the other components, except the catalytic subunits in chromatin remodeling, remain largely unknown (Narlikar et al., 2002).

Accumulating evidence revealed that both the chromatin-remodeling complexes and the coregulatory complexes cooperatively support transactivation of sequence-specific regulators like NRs (Glass and Rosenfeld, 2000; Emerson, 2002; Narlikar et al., 2002). However, the underlying molecular basis of the functional interplay among the complexes and the order of their recruitment through regulators to the promoters in controlling transcription at the specific local sites on the promoters are largely unknown.

Williams syndrome (WS) is a rare autosomal dominant hereditary disorder with multiple symptoms, including typically congenital vascular lesion, elfin face, mental retardation, and growth deficiency (Lu et al., 1998). Transient appearance of infantile aberrant vitamin D metabolism and hypercalcemia in the WS patients was also documented (Taylor et al., 1982; Garabedian et al., 1985). This syndrome is associated with genetic deletions at chromosome 7q 11.23, and several candidate genes in the deleted regions have been mapped from their mRNA expression levels (Hoogenraad et al., 2002). One gene, the Williams syndrome transcription factor (WSTF), has been suspected to be a candidate responsible for the diverse WS disorders (Lu et al., 1998; Peoples et al., 1998). This possibility is raised by the fact that WSTF is highly homologous to hACF1 as one of the WAC family proteins (Jones et al., 2000). Also, hACF1 is a partner of hSNF2h (a *Drosophila* ISWI homolog) to form well-characterized ISWI-based chromatin-remodeling complexes (Poot et al., 2000).

To search a chromatin-modifying complex to account for the ligand-independent occupancy of VDR in the target promoters, we purified from MCF7 cells a human multiprotein complex named "WINAC". The analysis of WINAC represents not only a molecular mechanism that a direct and selective interaction of a sequence-specific regulator with a chromatin-remodeling complex, but also the relationship between the function of WINAC and Williams syndrome disorders.

Results

Purification of a WSTF-Containing Multiprotein Complex Interacting with the VDR Ligand Binding Domain

To identify a coregulator complex for nuclear receptors, HeLa cell nuclear extracts were incubated with a chimeric VDR-DEF region protein (VDR-DEF) fused to glutathione-S-transferase (GST), in the presence or absence of 1α,25(OH)2D3 (Figure 1A). Proteins associated with VDR were collected under a milder washing condition (Yanagisawa et al. 2002) than that in the previous report (Rachez et al., 1998). Proteins that interacted with VDR-DEF were separated by SDS-PAGE and silver stained (Figure 1B). Mass spectrometry and the apparent molecular weights of the different proteins associated with the VDR-DEF in a ligand-dependent way led to the identification of several known components of the DRIP/TRAP/SMCC complex (Figure 1B), in agreement with previous observations (Rachez et al., 1998; Gu et al., 1999; Yanagisawa et al., 2002). One of the ligand-independent VDR-specific interactants was the Williams syndrome transcription factor (WSTF)/WBSCR9/BAZ1B (Lu et al., 1998; Peoples et al., 1998; Jones et al., 2000) (Figure 1B), and the WSTF protein was detected indeed in native HeLa cells (Figure 1C).

By Western blotting with specific antibodies, the NR coactivators, TRAP220 and TIF2, were detected only when VDR and ERα were liganded (Figure 1B). Unlike these factors, no ligand dependency, but VDR-selective interaction was found in WSTF (Figure 1B). By a GST pull-down assay, the physical and constitutive interaction of recombinant WSTF in vitro was observed for VDR-DEF irrespective of ligand binding, but not detected for ERα LBD (Figure 1D). In coimmunoprecipitations using the nuclear extracts of transfected MCF7 cells, WSTF appeared to interact with both unliganded and liganded VDR, while ligand-dependent recruitment of TRAP220 and TIF2 were expectedly seen for VDR as well as ERα (Yanagisawa et al., 2002) (Figure 1E).

To purify a WSTF-containing complex, we established a MCF7 stable transformant overexpressing FLAG-tagged WSTF. With the nuclear extracts of the stable transformants, WSTF containing complexes were isolated by multistep purification using the GST-VDR column and an anti-FLAG affinity resin column (Figure 2A). On the glycerol density gradient (Figure 2B, upper image), the purified complexes with a molecular weight of greater than 670 kDa bound to the GST-VDR column and these large molecular weight fractions contained WSTF, indicating that WSTF forms a stable nuclear complex. The fractions containing FLAG-tagged WSTF were then applied on the anti-FLAG affinity column to isolate the complex.

Identification of a WSTF Complex

With the mass fingerprinting, we identified all the components of the purified complex containing WSTF (Figure 2C), and designated this complex as WINAC (*W*STF *I*ncluding *N*ucleosome *A*ssembly Complex). WINAC stable formation was further supported by coimmunoprecipitation with a CAF-1p150 antibody (Figure 2C). WINAC consists of at least 13 components, but unexpectedly

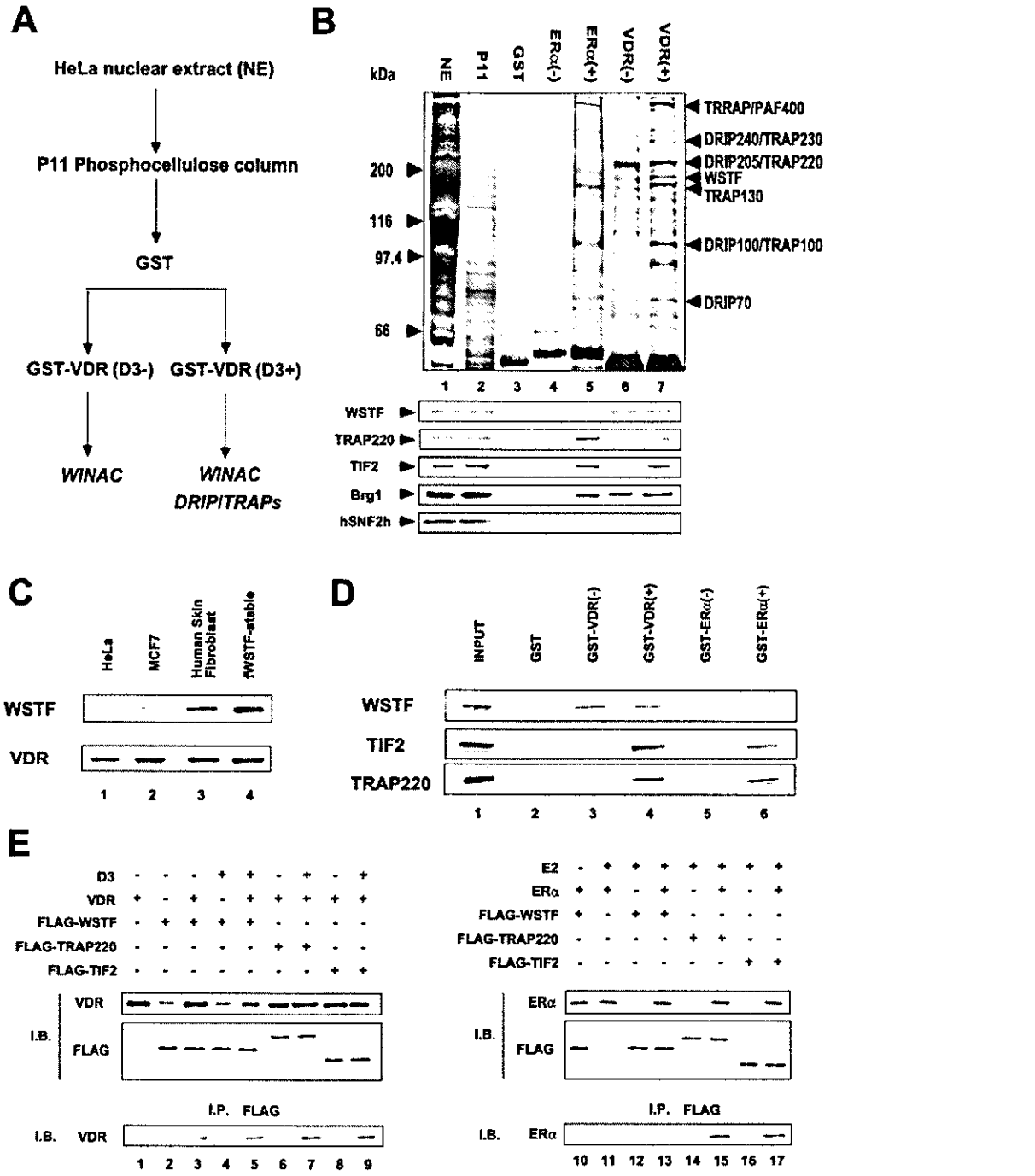

Figure 1. Purification and Identification of Human Proteins Interacting with 1α,25(OH)2D3, Unbound and Bound VDR

(A) Purification scheme for VDR interacting proteins. The eluted fraction from P11 phosphocellulose column was incubated with immobilized GST-VDR(DEF) in the absence or presence of 1α,25(OH)2D3(D3,10^{-6} M).

(B) Identification of ligand-independent and -dependent VDR interacting proteins. In the upper image, fractions were subjected to SDS-PAGE, followed by silver staining. Total HeLa S3 nuclear extract [NE] (lane 1), a fraction eluted from the P11 column [p11] (lane 2), fractions from GST [GST] (lane 3), unliganded- and liganded-GST-ERα(DEF) columns [ERα(−);ERα(+)] (lanes 4 and 5), unliganded- and liganded-GST-VDR(DEF) columns [VDR(−);VDR(+)] were examined by mass spectrometry and identified proteins are indicated at the right side of the image. The lower image shows Western blot analysis using specific antibodies shown in the image.

(C) Protein expression in cultured cells. Western blotting with antibodies against WSTF or VDR was performed with indicated cell lines (3 × 10^5 cells/lane).

(D) Direct and ligand-independent interaction of WSTF with VDR in vitro. WSTF, TIF2, and TRAP220 were translated in vitro and incubated with a receptor-GST chimeric protein immobilized on glutathione-Sepharose beads in the presence or absence of the cognate ligands.

(E) 1α,25(OH)2D3-independent interaction between VDR and WSTF in vivo. The upper image displays the Western blot of the total cell extracts (Yanagisawa et al., 2002) to verify expression. The lower image shows the Western blot of the immunoprecipitates by anti-FLAG M2-affinity resin to detect the receptor.

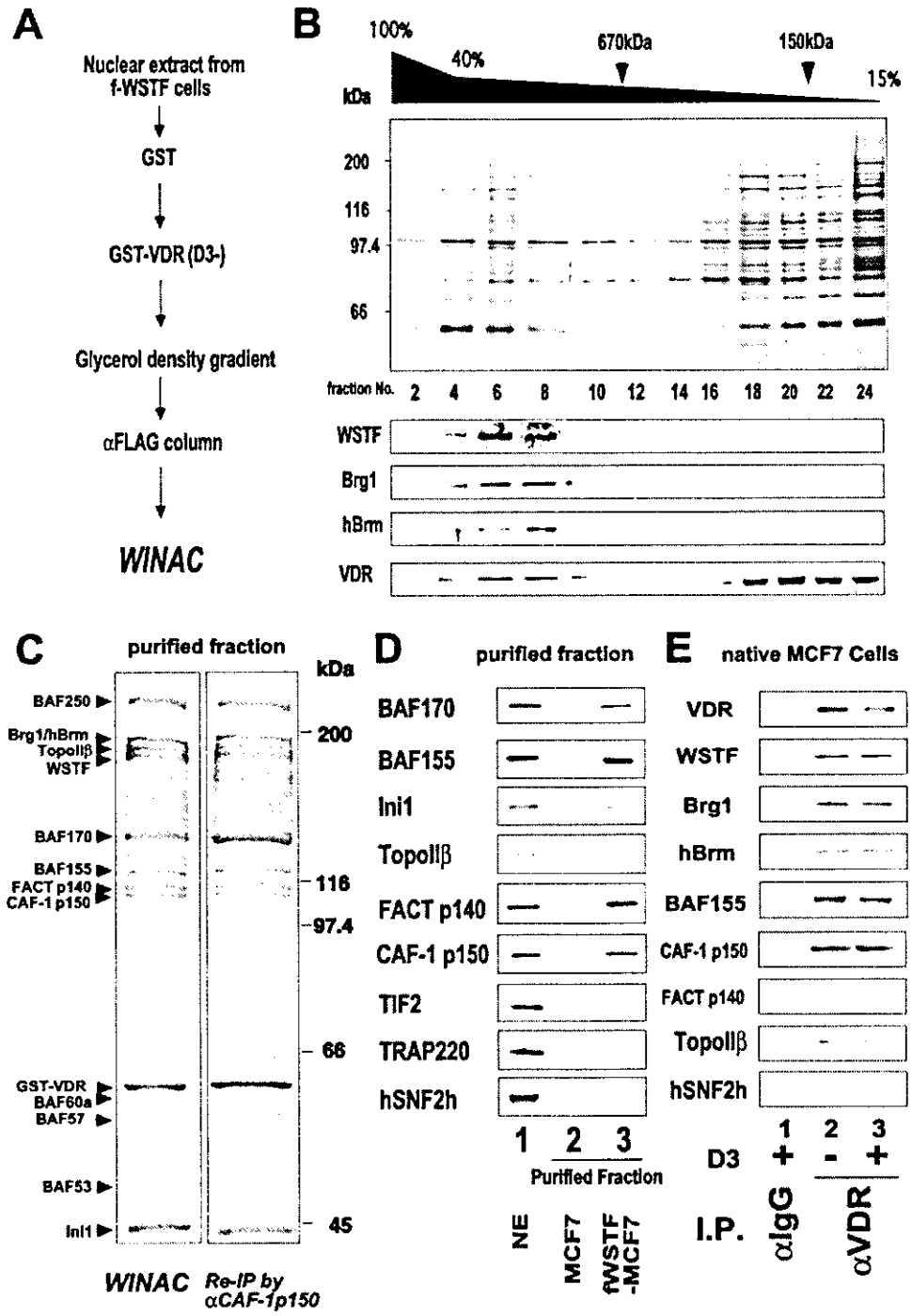

Figure 2. Purification and Identification of a Human WSTF-Containing Multiprotein Complex "WINAC"

(A) Purification scheme of WINAC from MCF7 stable transformants (Yanagisawa et al., 2002).

(B) Fractionation of purified complexes on glycerol density gradient. In the lower image, Western blot analysis of each fraction using specific antibodies is shown.

(C) The purified complex was subjected to SDS-PAGE, followed by silver staining and identified by mass spectrometry (left image). The right image shows the reimmunoprecipitation (Re-IP) of purified WINAC by the anti-CAF-1 p150 antibody.

(D) Western blot analysis of WINAC. Western blot analysis was performed to compare nuclear extracts (lane 1), mock MCF7 (lane 2), and FLAG-WSTF stable transformants containing WINAC (lane 3) with specific antibodies.

(E) Detection of endogenous WINAC components by Western blotting.

contains neither hSNF2h nor the components of known ISWI-based complexes (Figure 2C). Rather, the SWI/SNF type ATPases (Brg1 and hBrm) and several BAF components share with the SWI2/SNF2-based complexes (Narlikar et al., 2002). However, we could not detect BAF180, which is specific to one of the hSWI/